University of Washington

Abstract

Unlocking the Secrets of Slow Slip in Cascadia Using Low-Frequency Earthquakes

Justin R. Sweet

Chair of the Supervisory Committee:

Professor Kenneth C. Creager

Department of Earth and Space Sciences

Recent discoveries in subduction zones worldwide—including here in Cascadia—have illuminated the once shrouded process of plate convergence below the seismogenic zone. Early geodetic [*Dragert, et al.,* 2001] and seismic [*Obara,* 2002] signals were observed to correlate in space and time, and were associated with periodic episodes of deep slow slip, termed Episodic Tremor and Slip (ETS) [*Rogers and Dragert,* 2003]. In this dissertation, I present evidence further detailing the process of where, how, and how often deep slow slip occurs using several catalogs of low-frequency earthquakes (LFEs) as slow slip indicators. In the first section I compare four distinct LFE families that span the range of the ETS zone beneath western Washington State. I find that LFE behavior varies systematically with depth: LFE moments, swarm durations, and swarm recurrence intervals are all

largest in the updip portion of the ETS zone, and smallest in the downdip portion. I interpret these systematic differences as a result of variation in fault strength on the subduction interface—with the strongest coupling found updip (near the seismogenic zone), and the weakest coupling found downdip. In the second section I look within individual LFE families and perform double-difference event relocations to map out the spatial extent of the LFE patch (or patches) responsible for LFE generation. I determine LFE locking efficiency from estimates of LFE density and released seismic moment. I also track LFE migrations over time in an effort to map the progression of slow slip fronts, rapid tremor reversals (RTRs), and other phenomena.

TABLE OF CONTENTS

List of figures

List of Tables

I. Introduction

The Cascadia Subduction Zone (CSZ), stretching from northern California to northern Vancouver Island, is characterized by the subduction of the Juan de Fuca oceanic plate beneath the North American continental plate. At shallow depths, the interface between the two plates is locked and strain accumulates as the two plates converge, as evidenced by geodetic observations [*McCaffrey et al.,* 2007]. This locked zone is known to have ruptured in great megathrust earthquakes in the past, most recently in 1700 [*Satake et al.,* 1996]. Farther down the plate interface, below the bottom of the locked zone, the two plates slide past one another through a process of steady creep accommodated by higher temperatures, lower friction, and a possibly fluid-rich environment. The transition from full plate coupling in the locked zone to zero plate coupling at depth necessitates transitional modes of slip in-between, which are accommodated by pulses of slow slip. These pulses have slip speeds less than typical seismogenic slip speeds, yet have still been observed seismically through an assortment of new and exotic signals.

In the early 2000s a combination of advancing technologies like GPS, and increased seismic instrumentation revealed a new class of events related to slow slip. Episodes of slow slip were first noticed in the transition zone through use of GPS measurements [*Dragert et al.,* 2001]. A curious, emergent seismic signal known as tremor was reported shortly thereafter in the transition zone of a subduction zone beneath Japan [*Obara,* 2002]. A more complete picture emerged with the realization that seismic tremor and geodetically seen slow slip were part of the same phenomenon, termed Episodic Tremor and Slip (ETS) [*Rogers and Dragert,*

2003]. Since that time a whole suite of slow-slip-related events have been discovered, including short duration (1 s) events like low-frequency earthquakes (LFEs) [*Shelly et al.,* 2006], and longer duration (10s to 100s of seconds) very-low and ultra-low-frequency earthquakes (VLFs and ULFs) [*Ide et al.,* 2008; *Ito and Obara,* 2006]. Collectively these events fall under the term "slow earthquakes," so-called because they are related to slow slip and because they differ fundamentally from ordinary earthquakes in how their seismic moment scales to duration [*Ide et al.,* 2007].

Understanding how these slow slip phenomena occur is a crucial step in better understanding how plate convergence is accommodated within subduction zones. In Cascadia, historical records [*Miller et al.,* 2002] and recent monitoring [*Wech*, 2010] show that slow slip is periodic in nature, with different parts of the CSZ having different recurrence intervals. Beneath western Washington, the typical recurrence interval between large slow-slip events like ETS is about 14 months, while in northern California the average interval between ETS events is only about 6 months [*Brudzinski and Allen,* 2007]. Even for a given location like western Washington, slow slip events occur with differing regularity and size as a function of downdip distance [*Wech and Creager,* 2011]. Better understanding of where, how much, and how often slow slip occurs is necessary for mapping out where the transition zone ends and the locked zone begins—something of particular importance in estimates of seismic hazard for large urban centers like Portland, Seattle, and Vancouver.

In this thesis I analyze several families of low-frequency earthquakes (LFEs) to

study slow-slip in detail at specific locations on the plate interface beneath western Washington. The results are divided into two main sections. In the first I compare the activity of four different LFE families to see how slow-slip varies from place to place as a function of downdip distance. In the second I perform a detailed analysis of a single LFE family in an attempt to determine LFE patch sizes and stress drops. This latter analysis, which appears in chapter 3, has been published in *G-cubed* and can be found here:

Sweet, J. R., K. C. Creager, and H. Houston (2014), A family of repeating low-frequency earthquakes at the downdip edge of tremor and slip, *Geochem. Geophys. Geosyst*., 15, doi:10.1002/2014GC005449.

II. Variations in Cascadia LFE behavior with downdip distance

2.1 Introduction

The interface between the top of a subducting plate and the underside of the overriding plate—known as the plate interface—is a dynamic and scientifically interesting place. This interface can be simply divided into three primary regions: a shallow locked zone capable of storing and releasing vast amounts of strain energy in the form of megathrust earthquakes, a deep continuously-creeping zone that accommodates the convergence of the two plates without storing any strain, and a transition zone between the two that is capable of storing small amounts of strain that are released over timescales ranging from days to decades (Figure 2.S1). This transition zone is host to a variety of new seismically and geodetically observed phenomena including slow slip [*Dragert et al.,* 2001], tremor [*Obara,* 2002], episodic tremor and slip (ETS) [*Rogers and Dragert,* 2003], and low-frequency earthquakes (LFEs) [*Shelly et al.,* 2006]. In this study we analyze four LFE families that collectively span the width of the transition zone of the Cascadia Subduction Zone (CSZ) beneath western Washington State (Figure 2.1). The shallowest family (LFE1) lies at 36 km depth near the updip edge of the transition zone and is close to the updip edge of tremor locations in this part of Cascadia [*Wech et al.,* 2009]. The next two families (2 & 3) are at depths of 40 km and 44 km respectively, and lie roughly in the middle of the transition zone. The final family (LFE4) is the deepest family (46 km) and lies at the downdip end of the transition zone, just above the adjacent constantly-creeping zone.

2.2 Method

We created two catalogs for each of the four LFE families: 1) a long-term, single-array catalog, and 2) a short-term, multi-array catalog. The catalogs for each of our LFE families were built in the same manner as described in chapter 3. In each case, we chose a high amplitude signal during active tremor and used it as a reference event to build up a template. A 15-second window containing the P- and S-waves for the reference event is then auto-correlated with the surrounding 24 hours of data for all available channels from the 1-km aperture Big Skidder (BS) array of six 3-component stations to find matching events. This array is part of the Cascadia Arrays For EarthScope (CAFE) experiment. The resulting fully normalized auto-correlation functions—one for each channel—are then combined using a third-root stack to identify time windows that correlated best across all 18 channels. Templates are built by linearly stacking the 80 best correlating windows, forcing identical time offsets for each station/channel. This process is repeated 3 times to further improve the quality of the templates. A complete catalog is then produced using a stack of fully-normalized running auto-correlations between each stacked template and its corresponding continuous 5-year long seismogram. A fully-normalized auto-correlation is a normalized correlation coefficient determined at every time offset, varying between -1 and 1. For each day we calculate the median of the absolute deviation (MAD) of the stacked auto-correlation function. We define a detection as a time when the stacked auto correlation function exceeded 10*MAD and the mean correlation exceeded 0.275. Because the S minus P time is around 6 seconds, and there are often spurious detections when the P-wave of the template aligns with the S-wave of an LFE on the seismogram, we require the time between adjacent LFE detections

to be greater than 6 seconds. The resulting cleaned 5-year catalogs contained 632, 2081, and 3433 individual LFE detections for families 1 through 3 respectfully. For LFE family 4 we used the previously cleaned catalog from our earlier work, which also used a 10*MAD threshold with no correlation cutoff, and contained 8942 detections.

We also created catalogs for each of these 4 LFE families using multiple arrays during the Array of Arrays (AOA) experiment (2009-2011). These catalogs, like the single-array catalogs above, used reference events to build up templates. However, unlike the earlier catalogs, we combined fully normalized auto-correlation functions from 9 channels at each of 7 arrays (BH, BS, CL, DR, GC, PA, TB) using a third-root stack (Figure 2.1). The resulting stacked auto-correlation functions are more restrictive (and thus contain fewer detections) than those in our single-array catalogs because only detections that occur at exactly the same lag times across all the arrays will add constructively (Figure 2.S2). In this way, these multi-array catalogs allow us to search for LFE activity at very localized locations, rather than over a wider area (as in the case of our single-array catalogs).

2.3 Results

In an effort to quantify the size of the area over which our single-array catalogs identified matching events, we compared the single-array catalogs for our two most closely located LFE families (~12 km apart). In order to explore this, we relax our criteria to allow for more distant and lower-correlating events to be included. These uncleaned catalogs differ from our standard catalogs in that they keep detections below 0.275, which has the effect of keeping events that have lower SNR and which are farther

away from the centroid of the template event for that catalog. Over the 5-year period covered by the uncleaned catalogs for LFE families 2 and 3, we find 122 cases where both catalogs had detections within 0.2 s of each other, suggesting that these two catalogs are detecting the same events. All of these simultaneous detections had relatively low correlation values within their respective catalogs, always less than 0.4. The mean correlation value for all the detections within each of the uncleaned single-array catalogs is 0.35 ± .07, while the mean correlation value for the 122 simultaneous detections is 0.25 ± .06. We employed a double-difference relocation method [*Waldhauser and Ellsworth,* 2000] to find precise relative locations for events from families 2 and 3 as well as from the set of 122 common events from the suspected new family. For each channel, we bandpass filter between 2-8 Hz and auto-correlate waveforms to calculate differential times for each event pair. We use channels from all stations at each of several arrays, keeping the median value at each array to improve the accuracy of our time picks. We group events by their respective family (2, 3, and new) and compare the differential times of events from one group with another to find the dominant time lags between families. To remove noise, we only keep lags within 0.15 s of the dominant time lag for a given event pair from separate groups. Event pairs from the same group had dominant lags near zero. The resulting locations show tight clusters of events at the locations of families 2 and 3 and a larger cluster of locations corresponding to the 122 common events (Figure 2.2). These results suggest that lower correlating detections in our uncleaned single-array catalog can be up to 10-15 km distant from the LFE family epicenter, and also illustrate a potential method for finding new LFE families from existing families.

As observed in our prior analysis of LFE4 (chapter 3), individual LFEs from all families are almost entirely temporally clustered into swarms. We analyze these swarms over a range of timescales—days-to-months and minutes-to-hours—to see how their behavior varies among families. For a given family, on a days-to-months timescale, we define a swarm as a period during which there are at least 10 LFEs with no gaps greater than 80 hours between LFEs. Striking differences are seen in the number of LFE swarms, their durations, and their recurrence intervals, all of which vary systematically with downdip distance (Figure 2.3). In general, shallow/updip families have larger swarms (more events, longer durations, higher magnitudes) and larger recurrence intervals, while deep/downdip families have smaller swarms with shorter recurrence intervals (Table 2.1). *Wech and Creager* [2011] reported similar findings for tectonic tremor in the same part of Cascadia, with the largest tremor swarms updip, and smaller, more frequent tremor swarms downdip. Our results confirm their findings, and expand upon them by allowing us to track LFE activity (and accompanying slow-slip) at finer spatial (meters vs. kilometers) and temporal (seconds vs. minutes) scales. While the tremor and LFE catalogs both easily detect the large updip ETS events, the LFE catalog is able to detect smaller episodes of slow slip that are absent from the tremor catalog—particularly for LFE4 at the far downdip edge of the transition zone.

Beginning at the updip end of the transition zone, we find that LFE1 is primarily active only during large ETS events that occur regularly every 14 months in this part of Cascadia [*Rogers and Dragert,* 2003]. During the 5-year period of our single-array catalog, we detect 6 swarms of this LFE family—5 major swarms corresponding to each of the 5 ETS events during the period of our catalog, and 1 minor swarm that was part of

a large inter-ETS event in March 2010. Interestingly, we find that this minor swarm does not appear in the multi-array catalog for this family, suggesting that slow slip from this large inter-ETS event came close to (<10-15 km), but did not actually reach the location of LFE1. In each of the 5 ETS swarms, LFE activity persists over a period of 3-4 days with remarkable repeatability from one ETS to another. In all cases, a similar temporal pattern is observed: a frenzied initial period lasting ~90 minutes containing a very high rate of LFE occurrence, followed by short duration (12 min), high-amplitude bursts over the following days (Figure 2.S2). In all 5 cases, the time between these later bursts is seen to increase systematically over the following several days. In total we observe 45 of these later bursts over all ETS events, and in every instance these bursts occurred during periods of favorable tidal stressing (Figure 2.4). In contrast, the initial frenzy sometimes occurs during favorable tidal stressing, and sometimes not. None of the other 3 LFE families we analyze exhibit such complex and repeatable behavior.

LFE families 2 and 3, like LFE1, are detected during all 5 of the major ETS events, and are also frequently active during inter-ETS events. As we move downdip from LFE family 1 to 2 and LFE family 2 to 3 we see increasing numbers of swarms with shorter median durations and shorter median recurrence intervals (Table 2.1, Figure 2.3). LFE swarm durations are defined as the time between the 10^{th} and 90^{th} percentile events within a swarm. The differences between LFE family 2 and 3 are surprising given that their epicenters are only 12 km apart. Over that short distance the number of swarms doubles, and the median swarm duration drops by more than a factor of 3. Likewise, median recurrence intervals drop from 151 days at LFE2 to just 58 days at LFE3. We also find interesting differences between ETS swarms and non-ETS swarms for these

families. On average, ETS swarms at LFE families 2 and 3 last three times as long, and release 2 to 3 times the moment of inter-ETS swarms. Interestingly, nearly 80% of the total moment we observe at LFE2 is released during ETS swarms, while at LFE3, the figure is only 40% (Table 2.1). It should be noted that due to the large amount of tectonic tremor present during ETS events, background noise levels during these times are significantly higher than at other times. Because individual LFEs are small events with generally poor signal-to-noise, this increased noise means that our catalogs are likely missing a significant number of detections during ETS events. The fact that we observe increased LFE moment release despite this limitation suggests that individual LFEs from these 2 families are significantly larger during ETS swarms than at other times. As prior studies have shown, the area encompassing the locations of LFE families 2 and 3 contains some of the highest densities of tremor locations [*Wech et al.,* 2009; *Ghosh et al.,* 2012] and LFE families [*Royer and Bostock,* 2013].

At the bottom of the transition zone, LFE4 exhibits frequent and steady activity compared to the other 3 families updip. Seen on average every 8 days in the form of small, short duration swarms, this LFE family is the only one of the four we analyze here that is not clearly tied to ETS events. Swarms at LFE4 occur on average 7 to 52 times as often and have durations 12 to 75 times shorter than the other 3 LFE families (Table 2.1). This family occurs in isolation with no other known LFE families or associated tectonic tremor within 10 km. This fact was used to analyze this family in great detail without interference from other nearby families [*Sweet et al.,* 2014]. Because this family is so isolated, its single-array catalog is unlikely to be contaminated by nearby LFEs in the same way as for the other 3 families. Accordingly, we view the single-array and multi-

array catalogs for this family to be more or less interchangeable for the purposes of analyzing its spatiotemporal behavior. High-quality double difference locations show that half of LFE4 events occur within a 300-m radius circle and that the remaining half form an elongated cloud stretching 2 km in the direction of relative plate motion (chapter 3).

2.4 LFE Seismic Moment

In order to quantify the size of the individual LFEs from each family, we use data from multiple arrays to invert for band-passed seismic moment. For this portion of our analysis, we use our multi-array catalogs to ensure sufficient station geometry to obtain robust estimates of band-passed seismic moment. We deconvolve our data to displacement and apply a zero-phase band-pass filter from 2-8 Hz. For each array (6 to 10 stations per array) we determine the time corresponding to the peak S-wave amplitude on all the horizontal channels, only keeping channels where the maximum amplitudes occur at times within ±0.2 s of each other. Because we do not know the S-wave polarity from each LFE family to each array, we test each of 4 possible channel orientations (E-up/N-up, E-up/N-down, E-down/N-up, E-down/N-down) to find which produces the highest number of consistent arrival times for each LFE family/array pair (Figure 2.5). By comparing this result to the predicted S-wave polarization for a shallow thrusting source at the location of each LFE family we choose a channel orientation for band-passed moment estimation. In most cases the predicted polarization agreed with our best channel orientation, however in cases where they disagreed, we favored the predicted polarization. A recent study of LFE focal mechanisms in this part of Cascadia found that ~90% of events had double couple mechanisms consistent with shallow thrusting in the

direction of relative plate motion [*Royer and Bostock,* 2013]. We find the nearest local minima to either side of each S-wave maximum and calculate the area of the resulting triangles formed by these three points. This is an estimate of the time integral of the displacement pulse. We keep the median value of this integral for each array.

We use the following equation [from *Shearer*, 1999] for far-field S-wave displacement in an elastic whole space observed at position **x** from a source at **x**=0:

$$\mathbf{u}^S(\mathbf{x},t) = \frac{1}{4\pi\rho\beta^3}(\cos 2\theta \cos\phi\, \widehat{\boldsymbol{\theta}} - \cos\theta \sin\phi\, \widehat{\boldsymbol{\phi}})\frac{1}{r}\dot{M}_0(t-\frac{r}{\beta}) \qquad (2.1)$$

where β is the shear velocity, ρ is the density, and r is the distance from source to receiver. Because we integrate uniformly over ray directions, the mean S-wave radiation does not depend on the orientation of the double-couple source. We rearrange terms and integrate moment rate over time to solve for band-passed seismic moment (M_0):

$$M_0 = \frac{(4\pi\rho\beta^3)r}{Rc} e^{\frac{rf\pi}{\beta Q}} \int \mathbf{u}^S\, dt \qquad (2.2)$$

where $R = 2$ is a free-surface correction for near vertical incident rays, $c = 0.59$ is the average of the amplitude of the directional terms over the unit sphere, f is the dominant frequency for which attenuation is calculated, and Q is the S-wave quality factor. We chose a dominant frequency of 4 Hz and a quality factor of 200 for our calculations, in line with previous studies in this part of Cascadia [*Gomberg et al.,* 2012].

For the i^{th} source and j^{th} array, we augment equation (2.2) with a dimensionless array correction term (S_j) to account for local geology, and rewrite it as:

$$\ln M_i - \ln S_j = \ln C_{ij} + \ln D_{ij} \qquad (2.3)$$

where M_i is the band-passed seismic moment of the i^{th} LFE, S_j is the dimensionless station correction term for the j^{th} array, $C_{ij} = \frac{(4\pi\rho\beta^3)r_{ij}}{Rc} e^{\frac{r_{ij}f\pi}{\beta Q}}$ is known and the data D_{ij} is

the median of the time integral of the S-wave displacement. There are N_E (Number of LFEs) plus N_S (number of arrays) unknown model parameters on the left side of this equation and of order N_E times N_S observations to constrain them. We create a vector of $N_E + N_S$ model parameters and a vector of corrected data (sum of terms on the right had side) and relate them to each other by multiplying the model vector from the left by a matrix of ones and zeros so we can invert simultaneously for band-passed seismic moment and station corrections terms with the side constraint that the product of the array corrections equals 1. We find that error distributions are log normal for events from each of the 4 LFE families at each of 4 arrays used for the inversion. The means of these distributions are all near zero, and less than 0.4% of our 10,269 observations have errors $>\pm 0.5$. We inverted for moments using Q_s values ranging from 50 to 300 and found that our misfits and error distributions were insensitive to the choice of Q_s.

Using data from four different arrays and 192, 583, 1696, and 594 events from families 1 through 4 respectively, we find a systematic pattern of increasing LFE band-passed moment as you move updip (Figure 2.6). The largest median LFE moment magnitudes are seen at LFE1 (M_w1.66) and the smallest at LFE4 (M_w1.18), corresponding to a factor of ~6 difference in band-passed seismic moment. The largest individual events observed are seen at LFE1 (M_w1.9), while the smallest individual event observed are seen at LFE families 3 and 4 (M_w1.03 and M_w1.05) (Table 2.1). The larger minimum event sizes seen at LFEs 1 and 2 are likely a result of the increased noise levels present during ETS events when these two families are most active compared to relatively lower noise levels that occur during smaller inter-ETS swarms at LFEs 3 and 4. As mentioned previously, LFEs from swarms occurring during ETS events at LFE families 2 and 3 are significantly larger

than those seen during inter-ETS swarms. Similar comparisons for LFE families 1 and 4 are difficult because LFE1 is only observed during ETS events, and LFE4 seems largely unaffiliated with ETS events. If we analyze swarms at LFE4 that occur nearest to times of ETS updip, we do find that they have a larger median magnitude (M_w1.32) than for swarms occurring at other times (M_w1.17). However it is possible that this result is due to fewer detections of small LFEs during ETS periods because of increased noise levels. Site responses for the arrays ranged from 2-4.

The distribution of amplitudes for each of the four LFE families is best approximated by an exponential distribution, rather than a power-law distribution as commonly seen in ordinary earthquakes (Figure 2.7). This result has been previously seen in studies of tremor in Japan [*Watanabe et al.,* 2007], LFEs on the San Andreas Fault in California [*Shelly and Hardebeck,* 2010], and in our earlier paper on LFE4 [*Sweet et al.,* 2014]. The characteristic event size, which is determined by the slope of the exponential distribution for that catalog, is observed to vary from M_w1.85 for LFE1 to M_w1.25 for LFE4. For each family, the corresponding power-law distribution varies continuously at low amplitudes, and yields exceptionally high b-values between 3 and 5, suggesting that this is not the correct amplitude distribution.

2.5 Relative LFE Locations

In an effort to compare the sizes of the LFE-generating patches, we perform a double-difference relocation of several hundred of the highest correlating events from each of our 4 families [*Waldhauser and Ellsworth,* 2000]. These events are selected from the single-array catalog, but because the correlation values of the selected events are >0.4

these events are likely to lie closer to the family centroid, even though they come from our less restrictive catalog. One reason we chose to select events from this catalog instead of our multi-array catalog was a desire to see if individual LFEs from a given family clustered into single or multiple patches—something that may have been impossible to resolve with a more restrictive catalog. For each family, our data consisted of millions of autocorrelation-obtained differential times, measuring the time between P or S waves for all event pairs on a given channel. We used channels from several arrays as well as single stations to maximize our spatial coverage and improve the quality of our relocations. For stations within arrays, we stack autocorrelations between events across all array channels to improve our lag time picks. Additionally, we only keep lags ±0.15 s from the most commonly measured lag (Figure 2.S3) to maximize our signal and minimize inclusion of noise. We find a variety of location distributions across our four LFE families (Figure 2.8, Figures 2.S4-7). Most families show a central core with high LFE densities—likely corresponding to the hypocentral location for that LFE template—surrounded by a cloud of lighter densities. At least some of these lower-density locations are in fact real, as seen at LFE4 [*Sweet et al.,* 2014], though others are undoubtedly mislocated events from the central core. LFE3 (Figure 2.S6) appears to have two high-density cores separated by about 1 km with lesser densities of LFEs between. LFEs 2 and 4 (Figures 2.S5, 2.S7) show elongation of LFE distributions parallel to the plate convergence direction, suggesting shear slip between the plates is somehow governing and/or influencing the generation of LFEs at these locations. LFE3 may show a hint of convergence parallel elongation as well, though the trend is less clear. In cross section (Figure 2.8) we note that for the two LFE families most-directly beneath our arrays (2 &

3) the depth distributions collapse to very narrow surfaces and/or planes, with dips generally consistent with the eastward-dipping JdF-NA plate interface. Perhaps unsurprisingly, the depth distributions for our other 2 LFE families are less planar, likely owing to their location outside the area of maximum station coverage. Compared to three different plate interface models, it appears that our LFEs most closely follow the depths of [*McCrory,* 2012].

2.6 Discussion

The combined time histories and seismic moment measurements from four LFE families indicate that LFE behavior on the plate interface is strongly influenced by depth. The largest LFE moments, swarm durations, and recurrence intervals are all found at our shallowest LFE family and decrease systematically with increasing distance downdip (Table 2.1). If we make the assumption, as others have [*Ide et al.,* 2007], that LFEs are driven by slow slip on the plate interface, then we should expect similarly large, and infrequent pulses of slow slip to occur in the shallowest portion of the transition zone. Geodetic observations [*Wang et al.,* 2008; *Schmidt and Gao,* 2010; *Bartlow et al.,* 2011] confirm these suspicions, and indicate that the largest slow slip episodes accommodate up to 2-4 cm of slip over a period of several weeks [*Wech et al.,* 2009]. In contrast, at the downdip end of the transition zone, we find the smallest LFE moments, swarm durations, and recurrence intervals—implying that slow slip at these depths is frequent, and much smaller in magnitude and extent. Between the top and bottom of the transition zone, the size, duration, and recurrence interval of LFE swarms is seen to systematically decrease,

which suggests some depth-dependent constraint is modifying LFE (and slow slip) behavior.

We favor the interpretation of *Wech and Creager* [2011], who proposed a friction-controlled stress transfer model to explain the similar differences in behavior of tectonic tremor swarms in this part of Cascadia. As with our LFE swarms, they noted the largest tremor durations and recurrence intervals were found on the shallow portion of the transition zone, and that these values systematically decrease as you move downdip. They explained this systematic variation through use of a stress transfer model, driven from below by the continuously-creeping zone just downdip of the transition zone (Figure 2.S8). In this model, stable creep loads the downdip portion of the transition zone, which has weaker fault coupling due to increased temperatures. Each slow slip episode relieves the local stress and transfers it updip to a portion of the transition zone that is more strongly coupled, and therefore has a higher stress threshold. Through a self-similar process, this model can explain the observations of small, frequent slow slip episodes downdip transitioning to large, infrequent slow slip episodes updip. Because tectonic tremor and LFEs are closely related [*Shelly et al.,* 2006], it is not surprising that our LFE results mirror the earlier results of *Wech and Creager* [2011]. However, unlike tremor, LFE analysis allows us to more accurately locate the depth of slow slip to very near the plate interface, and to show how these slow slip episodes evolve over shorter timescales, revealing details unseen in earlier work.

Comparisons between LFE catalogs and the tremor catalog for this part of Cascadia [*Wech,* 2010] reveal good agreement for large and intermediate slip events. Nearly all of the detections at LFE1 (ETS) and LFEs 2 and 3 (ETS and inter-ETS) are

corroborated by activity in the tremor catalog at the same times and locations. However, at the downdip edge of the transition zone near LFE4, the tremor catalog only detects a small fraction (<5%) of the events seen at LFE4. The isolated nature of LFE4 implies that most of the slip in the vicinity occurs aseismically, and thus the lack of detectable tremor in this area is to be expected. The lack of tremor does not indicate a lack of slow slip, however, and the activity at LFE4 indicates there are many more slow slip events downdip than inferred by *Wech and Creager* [2011].

The patterns of activity at our shallowest LFE family indicate a remarkably complex pattern of slow slip behavior at the updip end of the transition zone. During each of the 5 ETS events in our catalog, LFE1 shows two distinct phases of activity: an initial frenzy, followed by several short bursts. We interpret the initial frenzy, with its high rate of LFE detections, to represent the passage of the slow slip front at the location of our LFE family on the plate interface. Large slow slip episodes (ETS) are commonly observed to migrate along strike at speeds of 7-12 km/day [*Houston et al.,* 2011]. The high rate of LFE detections observed during the passage of the slow slip front agrees with several models of ETS that predict high slip rates to accompany the leading edge of slow slip [*Rubin,* 2011]. Following the initial frenzy, the activity at LFE1 transitions to short duration, high amplitude bursts, which have a systematically increasing recurrence interval (Figure 2.9). The observation that all of these later bursts occur during periods of favorable tidal stressing suggests that the plate interface is extremely weak following the passage of the slip front, similar to observations of tidal sensitivity of tremor and the interpretation of *Houston* (2014, submitted). In contrast, the initial frenzy that accompanies the passage of the slip front does not appear to be as sensitive to tidal

forcing—sometimes occurring during favorable stressing, sometimes not. The implication here is that the plate interface is more strongly coupled prior to the passage of the slip front. Immediately after the passage of the slip front, short bursts occur on average every few hours, but a few days later, the bursts may be separated by a day or more of quiescence. This observation could indicate healing or strengthening of the fault in the days following the passage of the slip front. *Thomas et al.* [2013] have shown that at least some of these later LFE bursts are correlated in time with known rapid tremor reversals (RTRs), which propagate rapidly backwards from the direction of the advancing slip front [*Houston et al.,* 2011]. As the slip front propagates farther away from the location of our LFE family, it is possible that in addition to fault healing, the increasing distance between the slip front—where RTRs typically initiate—and the LFE family means that fewer RTRs are able to propagate back to its location, thereby increasing the interval between short LFE bursts. *Rubin and Armbruster* [2013] track the motion of updip slow slip just north of our LFEs in southern Vancouver Island, and show dozens of backpropagating RTRs occurring in a small area (7 x 7 km) over the course of a single ETS event. It is likely that a similar process occurs at the location of our shallow family, LFE1.

Recent lab experiments by *Kaproth and Marone* [2013] using rock types thought to exist near tremor and slip on the plate interface reveal patterns of stick slip behavior reminiscent of activity seen at LFE1. In particular, their results show displacement histories (Figure S2.9) that look very similar to the 5-day counts seen in large ETS swarms at LFE1. They find that slip begins with a high rate of initial displacement, followed by decreasing activity—just like the detection rates at LFE1. Furthermore, this

finding is consistent with the asymmetric slip pulse posited by *Rubin* (2011), and asymmetric tremor distribution relative to start of tremor and slip front observed by *Houston* (2014, submitted). This similarity between our LFE observations and model results provides additional support for the notion that LFEs are the result of shear slip on the plate interface.

While slow slip during ETS events occur over wide areas and are large enough in magnitude to be detected geodetically [*Dragert and Wang,* 2011], smaller episodes of slow slip, and accompanying LFEs and tremor, are seen with regularity in our catalogs. LFE families 2 and 3 are most-optimally located to record these inter-ETS slip episodes, owing to their location in the middle of the transition zone (Figure 2.1). Situated only 12 km apart, LFE families 2 and 3 are surprisingly different given their close proximity. According to our long-term, single-array catalog, the deeper family (LFE3) is active in slow-slip-induced swarms more than twice as often as LFE2. The median duration of those swarms is about 3 times less than for typical swarms at LFE2. Likewise, the recurrence interval at LFE3 is 3 times shorter than at LFE2. In the context of a friction-controlled stress transfer model [e.g. *Wech & Creager,* 2011] these large contrasts over relatively short distances argue for a large frictional gradient between LFEs 2 and 3. Interestingly, these two families are located in a region of high tremor density, and near so-called tremor asperities [*Ghosh et al.,* 2012]. Also of note is the fact that at both LFE families 2 and 3, the median swarm duration and magnitude (M_w) is significantly larger during ETS-affiliated swarms, than during inter-ETS swarms. Perhaps not surprisingly, this indicates that the episodes of slow slip responsible for driving LFE swarms are larger in area and magnitude during ETS events than at other times.

The distribution of LFE locations suggests that shear slip between the plates influences LFE generation. The elongation of location distributions parallel to the plate convergence direction (Figures 2.S5-7), as well as the narrow, planar depth distribution of LFEs beneath our arrays (Figures 2.S5-6), both suggest that these LFEs lie on or near the plate interface and are influenced by shear slip in the plate convergence direction. LFE generation appears to be highly concentrated in path cores of dimension 300-500 m radius, with at least one family showing evidence for multiple patch cores. The patchy nature of LFE locations could indicate that only certain portions of the plate interface can radiate seismically while slipping. In this view, LFEs represent the seismic signature of slow-slip-driven sticky spots on the plate interface which are separated by aseismic or less-seismic regions. We see some evidence for propagating slow slip in patterns of LFE migration (Figure 2.10) at our dual-core family LFE3. Over a period of approximately 1 hour, LFE locations are observed to migrate ~2 km from east to west (updip) crossing from one patch core to another. Propagating slow slip fronts, like those observed by *Rubin and Armbruster* (2013), may be present at all four of our LFE families, but they are difficult to image if they have high velocities and/or if the rate of LFE generation is low.

2.7 Conclusions

In summary, we find that LFE behavior varies systematically with depth. LFE moments, swarm durations, and swarm recurrence intervals are all largest updip and smallest downdip. During ETS, LFEs 1 and 2 have activity continuing for 3 days, but at LFE3, only 35 and 12 km distant respectively, the activity ends after only 1.5 days.

Within LFE families 2 and 3, swarms contain 15-30% more moment and last 3-4 times as long during ETS events—suggesting greater amounts of slip than during inter-ETS events at these locations. In contrast, LFE1 does not appear to be active outside of ETS events, and activity at LFE4 seems not directly tied to large ETS events updip. We prefer a friction-controlled stress transfer model [e.g. *Wech and Creager,* 2011] to explain the variations we see in LFE behavior. We interpret the two distinct phases of activity seen at LFE1 as the passage of a slip front followed by short, tidally-modulated pulses of slow slip, perhaps related to RTRs propagating back from the advancing slip front. Double difference locations reveal that individual LFEs from each family locate in tight clusters near the plate interface and are often elongated parallel to the plate convergence direction in map view. Simultaneously-detected low-correlating events seen in catalogs of nearby LFE families 2 and 3 appear to be associated with a new LFE family located between the existing families—hinting at a possible method for finding new families from existing ones.

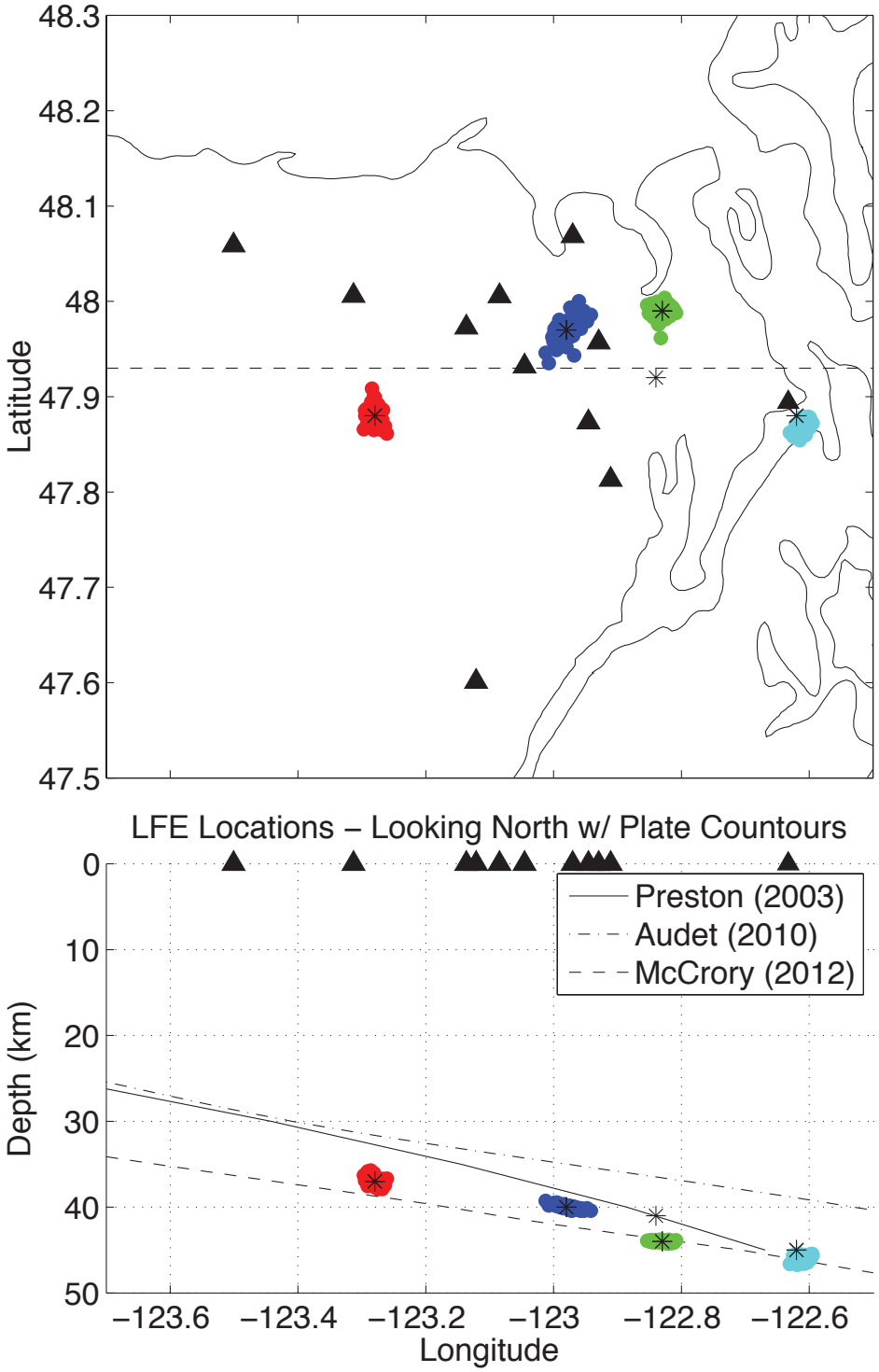

Figure 2.1 – Map and cross section showing the double-difference location clouds for each of the 4 LFE families, absolute locations determined from template waveforms (stars), stations and arrays used for locations (triangles), and three independent plate interface models (lines). From west to east the LFEs are: LFE1, LFE2, LFE3, and LFE4. A new LFE family between LFE2 and LFE3 is indicated by an additional black star.

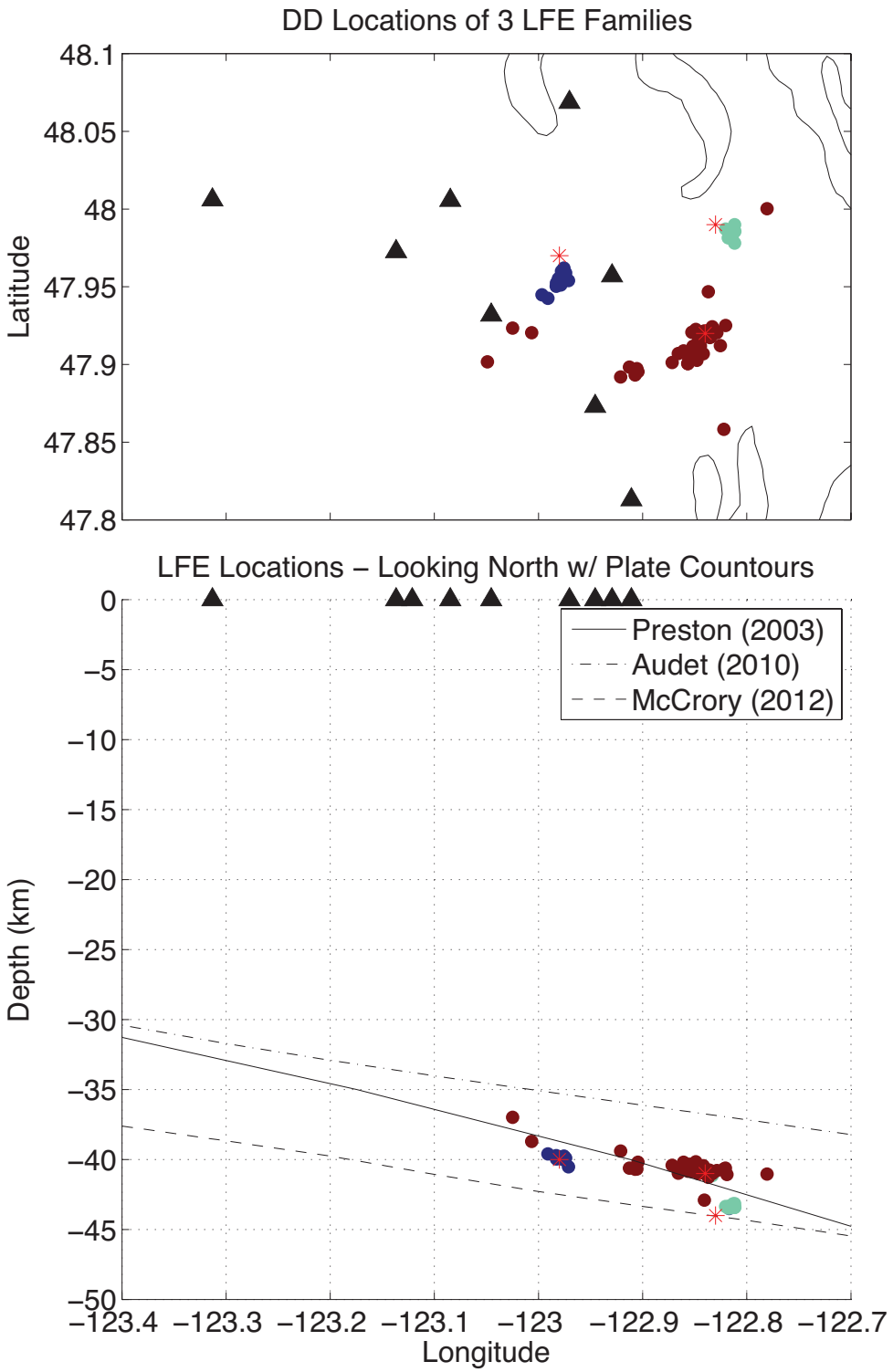

Figure 2.2 – Map and cross section showing a small number of relocated events from LFE2 (blue dots), LFE3 (cyan dots) and a new LFE family (brown dots). Red stars show the initial absolute locations of each of the 3 families. Black triangles denote stations or arrays. Three independent plate interface models are shown as solid or dashed lines in the cross section.

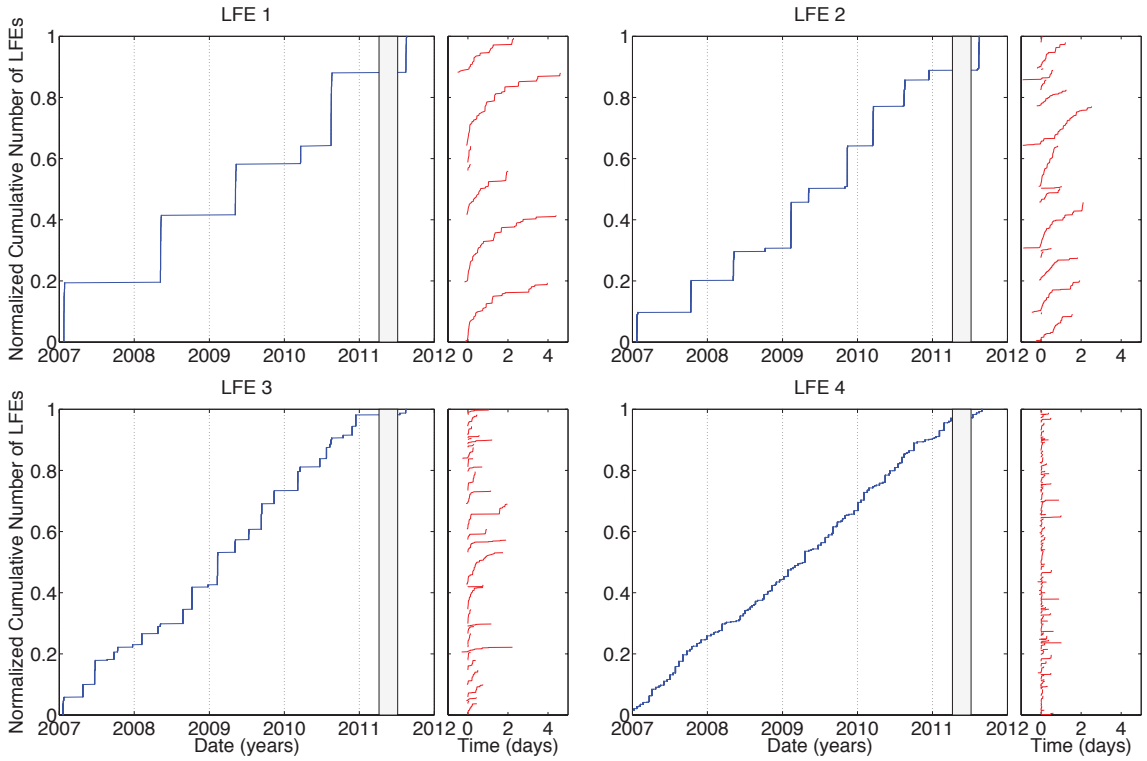

Figure 2.3 – Cumulative number of LFE detections versus time (blue lines) from our cleaned single-array catalog spanning 2007-2011. Vertical jumps corresponding to LFE swarms. The red lines to the right of each plot show a blown up view of each of the swarms over a period of 5 days. Vertical grey bars represent a data gap. Note that swarms occur more frequently downdip than updip, and that swarm durations are longer updip than downdip.

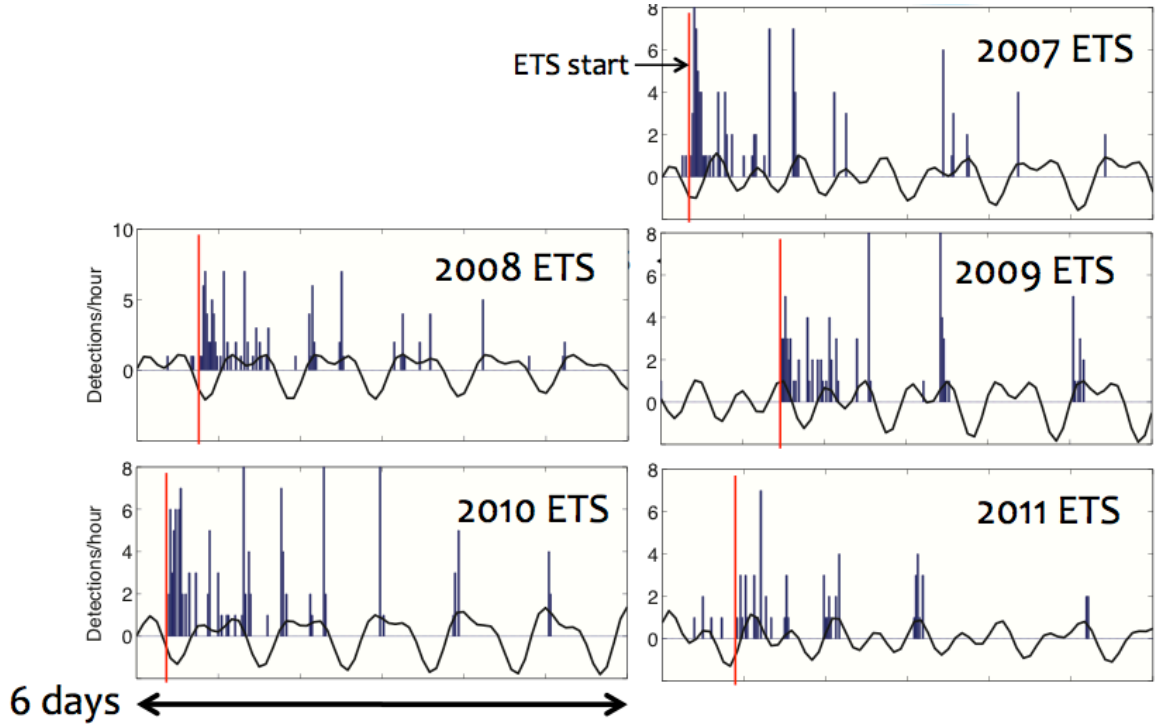

Figure 2.4 – Histograms of LFE1 detections per hour for 5 ETS events. The red line marks the onset of the ETS at LFE1. The black line indicates the magnitude of the encouraging tidal shear stress for slip in the direction of relative plate motion on the plate interface; positive is encouraging shear stress and negative is discouraging. Note that after the initial frenzied beginning, 100% of LFE1 detections occur during periods of encouraging tidal stress.

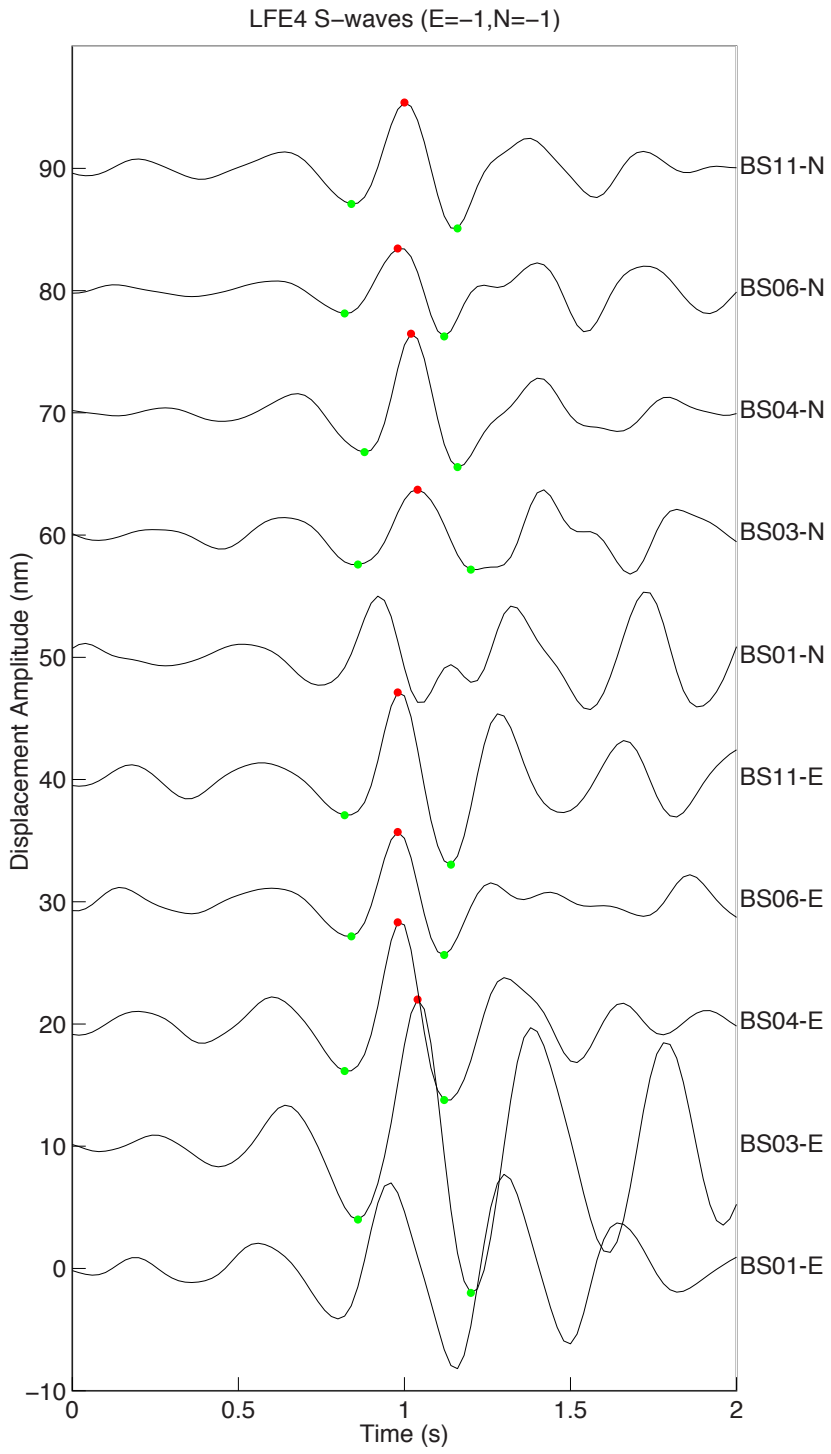

Figure 2.5 – Example of horizontal component S-wave displacement seismograms from the BS array with both East and North components flipped upside down to achieve optimal orientation for moment estimation. Red dots mark the location of maximum S-wave amplitude. Green dots mark the beginning and ends of our S-wave arrivals. Moment is estimated from the median area of the triangles formed by connecting the 3 dots in each trace. Traces without dots had maximum S-wave amplitudes more than 0.2 s from the median S-wave maximum time and were not used for moment estimation.

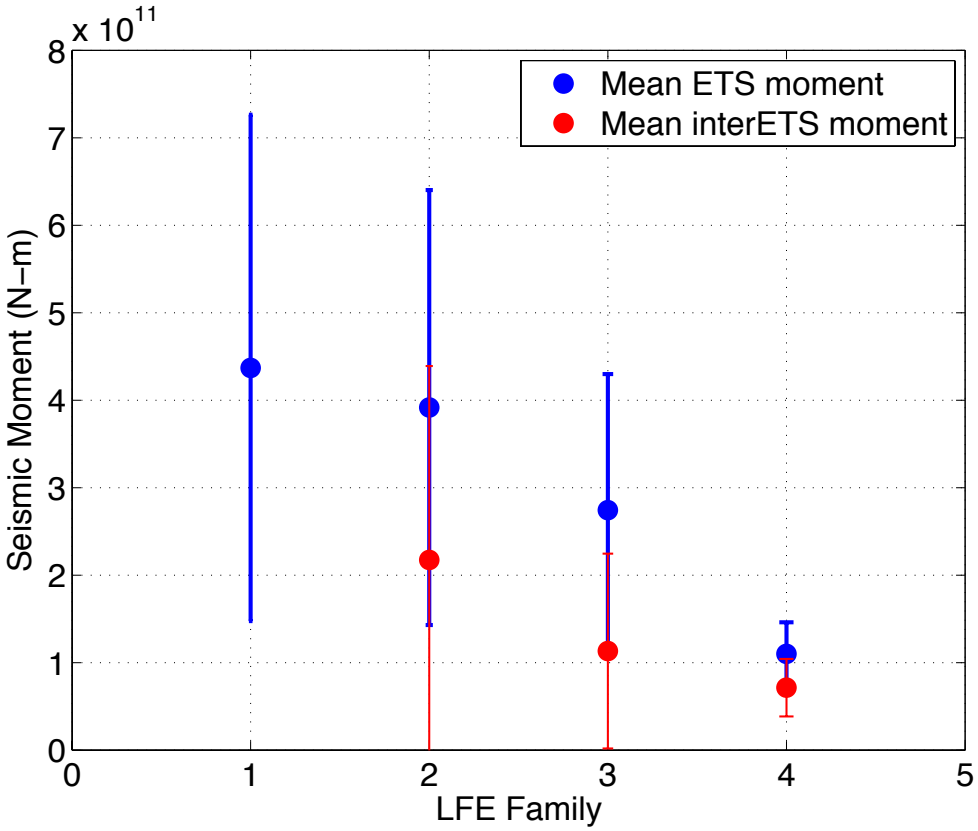

Figure 2.6 – Mean event moment and standard deviation by family for ETS swarms (blue) and interETS swarms (red). Note that at LFEs 2 and 3, ETS swarms tend to be significantly larger than interETS swarms.

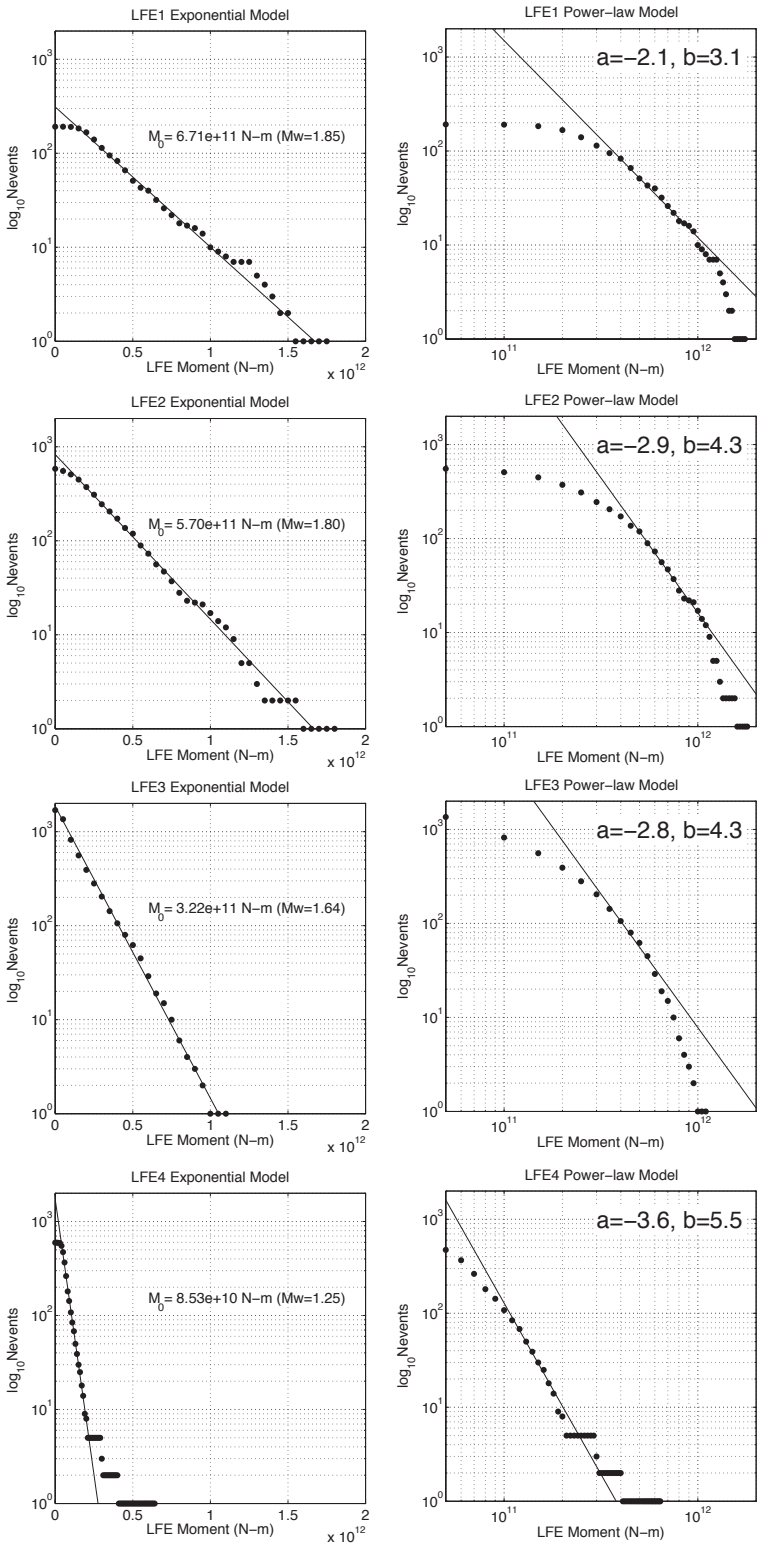

Figure 2.7 – Amplitude distributions (exponential left, power-law right) for each of our four LFE families. Note that characteristic event size, as measured by the slope of the plots on the left, varies continuously from LFE1 (M_w1.85) to LFE4 (M_w1.25). B-values range between 3 and 5.

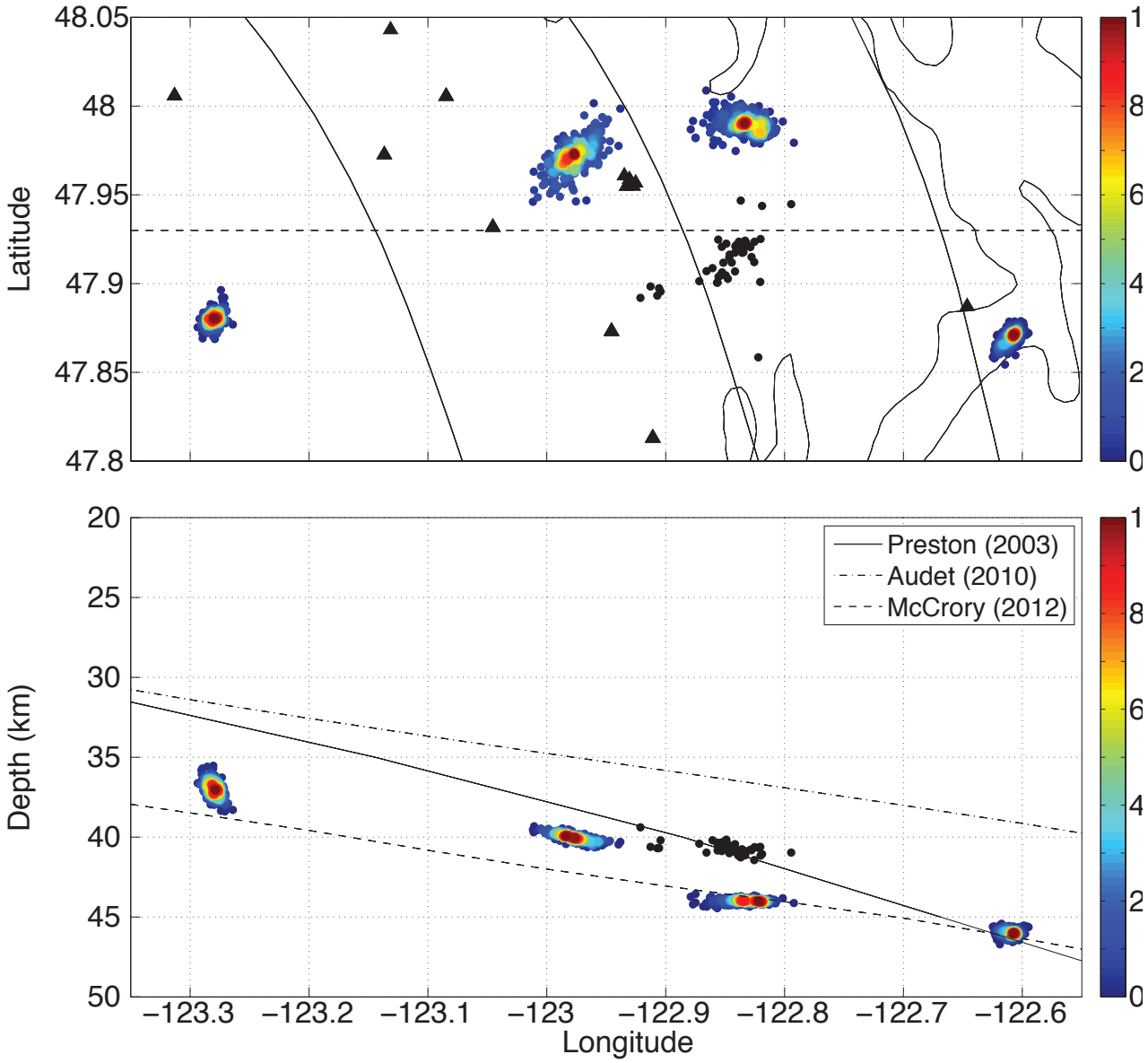

Figure 2.8 – Map and cross section showing relocated events from each of 4 LFE families colored by relative LFE density. LFE locations for a potential new family are plotted as black dots. Note that in map view several LFE families have elongated distributions that parallel the plate convergence direction, and that in cross section, the distributions are extremely narrow vertically, most notably for the 2 LFE families located most directly beneath our stations. It is likely that relocated events from LFEs 1 and 4 also have very narrow depth distributions but have poor relocations owing to their locations outside our network of stations and arrays.

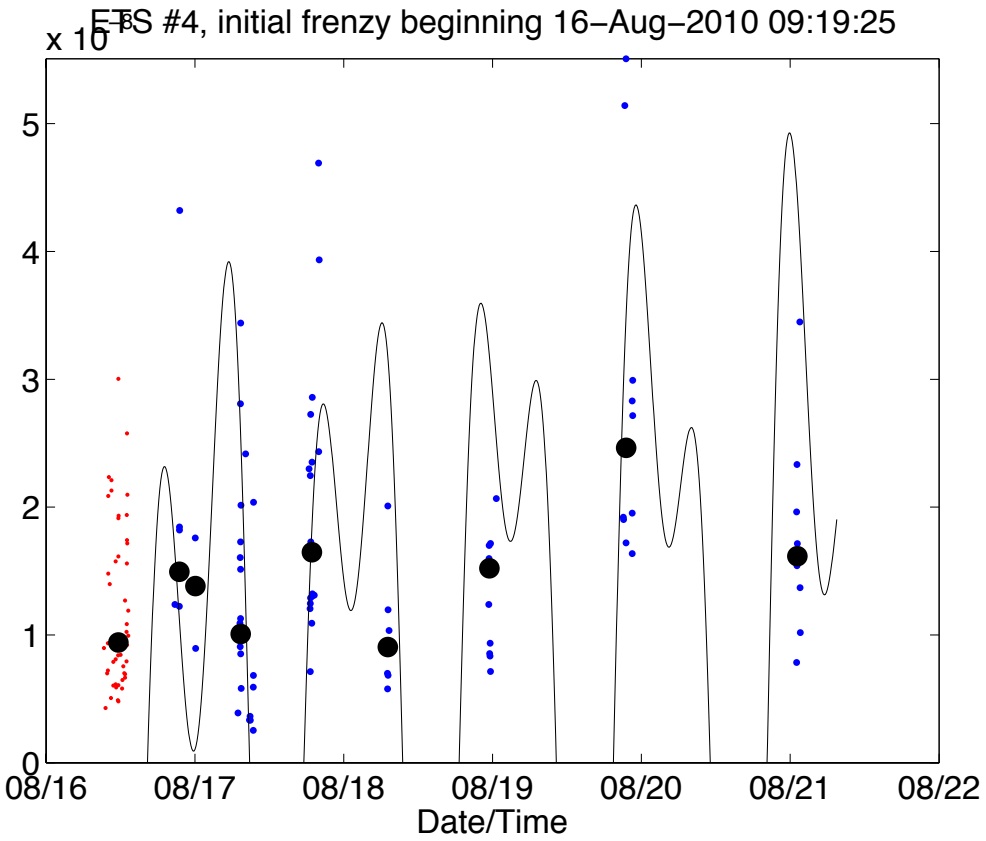

Figure 2.9 – Plot of event amplitudes during the 2010 ETS at LFE1. The events comprising the initial frenzy (red dots) have a lower median relative amplitude (black dots) than the median relative amplitudes seen for later bursts (blue dots). Tidal shear stress in the direction of plate convergence (black line) is observed to correlate with each of the short bursts after the initial frenzy.

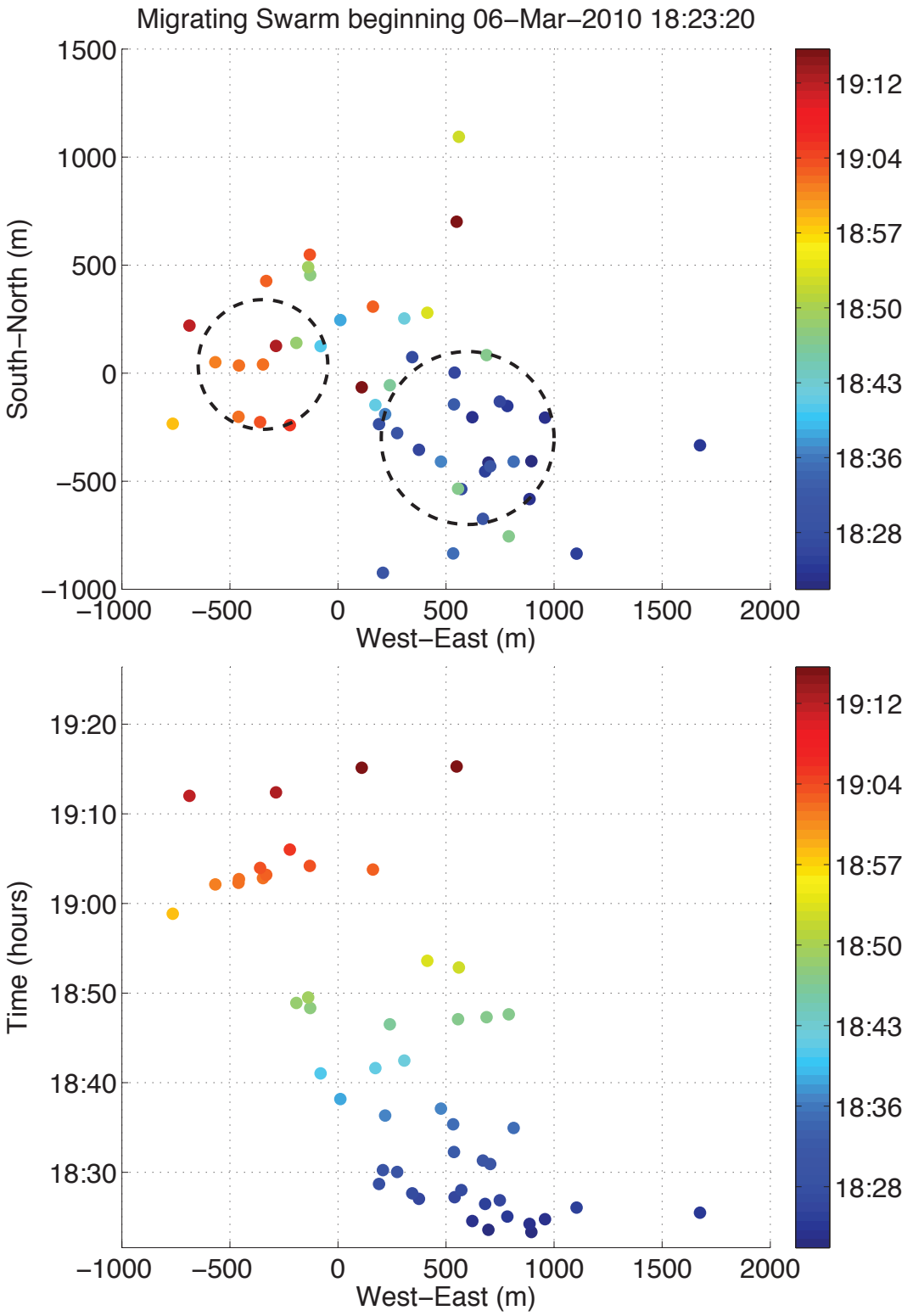

Figure 2.10 – Migration of LFEs seen in map view (top) at LFE3. LFE3 high density cores (dashed circles) illustrate where the migration is relative to the overall distribution (Figure 2.S6). East-West migration vs time (bottom) indicates migration velocity of ~2 km/hr.

	LFE1	LFE2	LFE3	LFE4
SINGLE-ARRAY CATALOG STATISTICS				
Total Events (uncleaned)	2047	5612	8493	9632
Total Events (cleaned)	632	2081	3433	4206
Number of swarms	6*	12	29	198
mean recurrence (days)	416	151	58	8
median duration (hours)	70	37	12	1
median ETS swarm duration (hours)	75	72	34	0.9
median non-ETS swarm duration (hours)	3*	23	9	1.2
MULTI-ARRAY CATALOG STATISTICS				
Total Events	192	583	1696	594
median (Mw)	1.66	1.58	1.29	1.18
mean (Mw)	1.67	1.55	1.31	1.20
90^{th} percentile (Mw)	1.90	1.84	1.63	1.37
10^{th} percentile (Mw)	1.48	1.22	1.03	1.05
ETS median (Mw)	n/a	1.63	1.56	1.32
non-ETS median (Mw)	n/a	1.40	1.23	1.17
% of total moment (ETS)	100%	77%	40%	13%
% of total moment (interETS)	0%	21%	59%	76%

Table 2.1 – Single-array catalog statistics for each of the four LFE families (top), and multi-array amplitude statistics (bottom). Single-array catalog swarms (2007-2011) were defined as at least 10 LFE detections with no gaps greater than 80 hours between them. Multi-array catalog swarms (2009-2011) were defined as at least 4 LFE detections with no gaps greater than 1 hour between them. *Note: LFE1 has a single non-ETS swarm in the single-array catalog that does not appear in the corresponding multi-array catalog, likely because this slow slip event came close to, but did not quite reach, the family centroid.

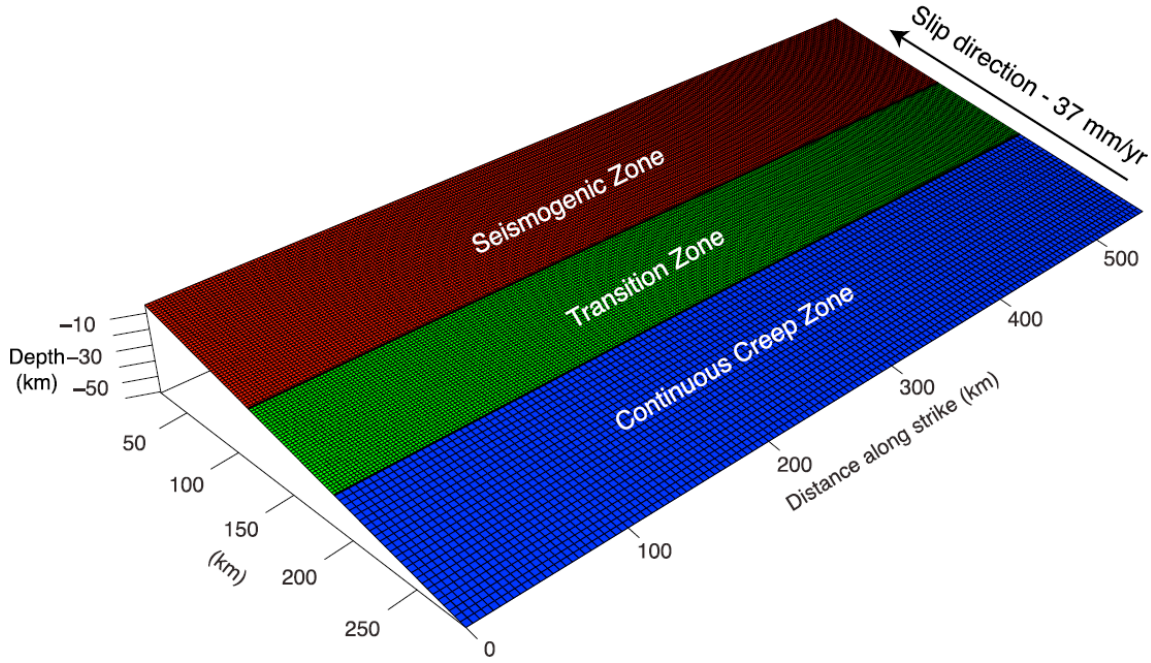

Figure 2.S1 – Simplified plate interface model space from *Colella et al.* [2012] showing the idealized distributions of a shallow seismogenic (locked) zone, an intermediate transition zone, and a deep continuously creeping zone.

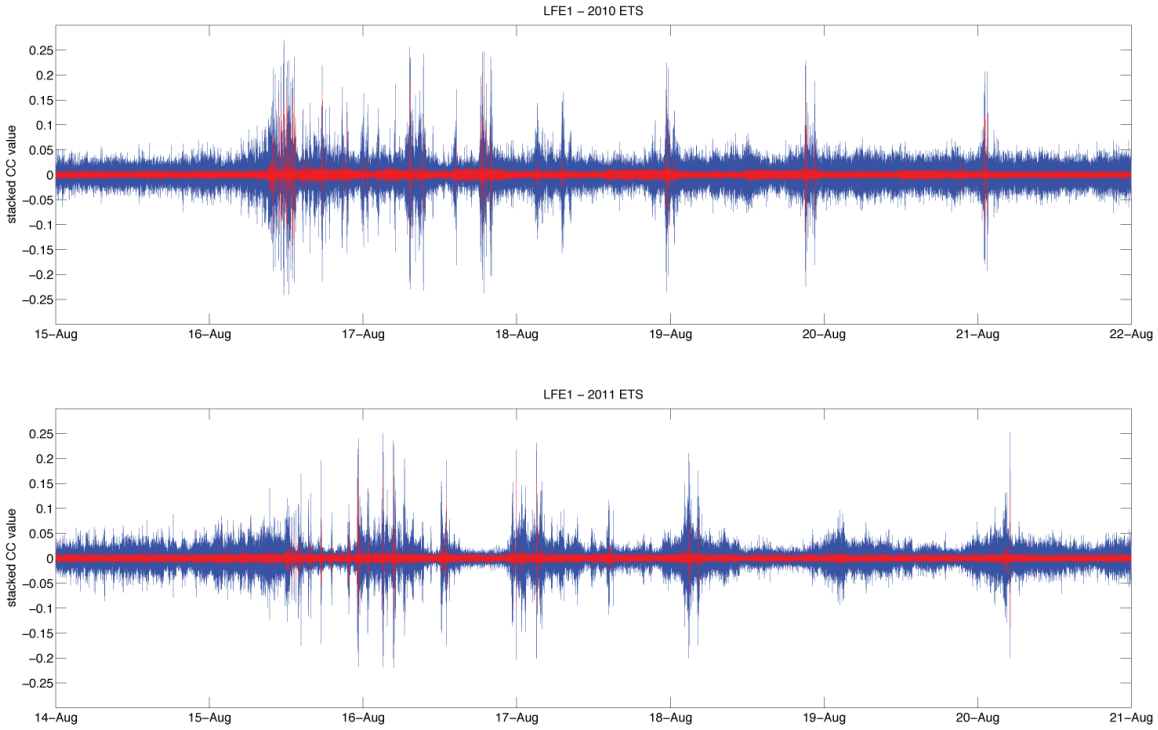

Figure 2.S2 – Stacked cross correlation functions for LFE1 using channels from a single array (blue) and multiple arrays (red) for the 2010 ETS (top) and 2011 ETS (bottom). In both plots the single array stacked cross correlation function (blue) is more "fuzzy" because it is detecting LFEs over a larger area than the more precise multi-array stacked cross correlation (red). The slow slip front passage can clearly be seen in the increased density of high correlations on 16-Aug during the 2010 ETS (top). The strong tidal modulation of LFE activity at and near LFE1 is evident between 16-Aug and 21-Aug during the 2011 ETS (bottom).

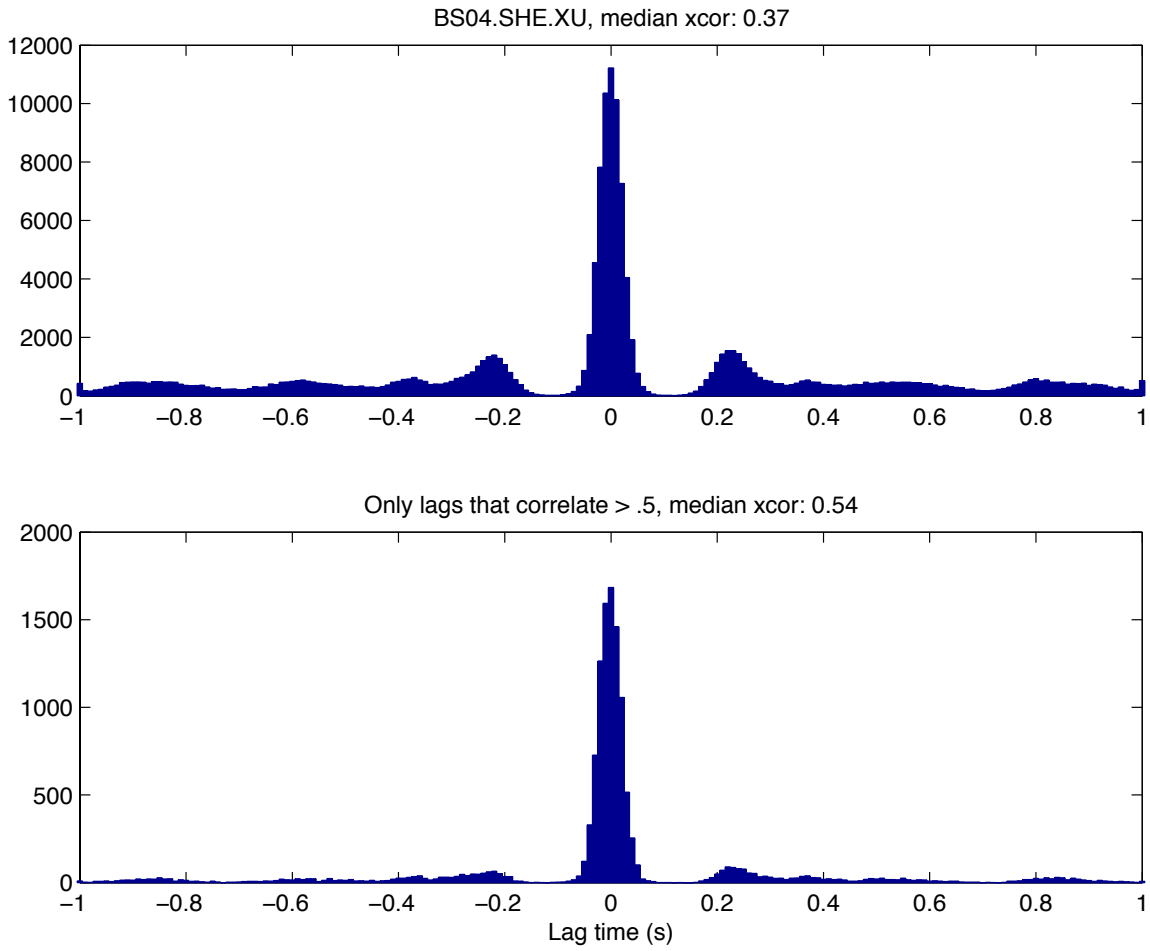

Figure 2.S3 – Histogram of lag times from cross correlation of event pairs from a single LFE family at station BS04. The large central peak, and symmetric nature of secondary peaks (likely due to cycle skips), along with the fact that there are almost no lags between ±0.2 s and the central peak, give us confidence that most of the lags ≥0.2 s are likely noise. Note how the side lobes are significantly diminished, relative to the central peak, if we only consider lags which correlate >0.5 (bottom plot). We keep lags within ±0.15 s of zero for event relocation using hypoDD.

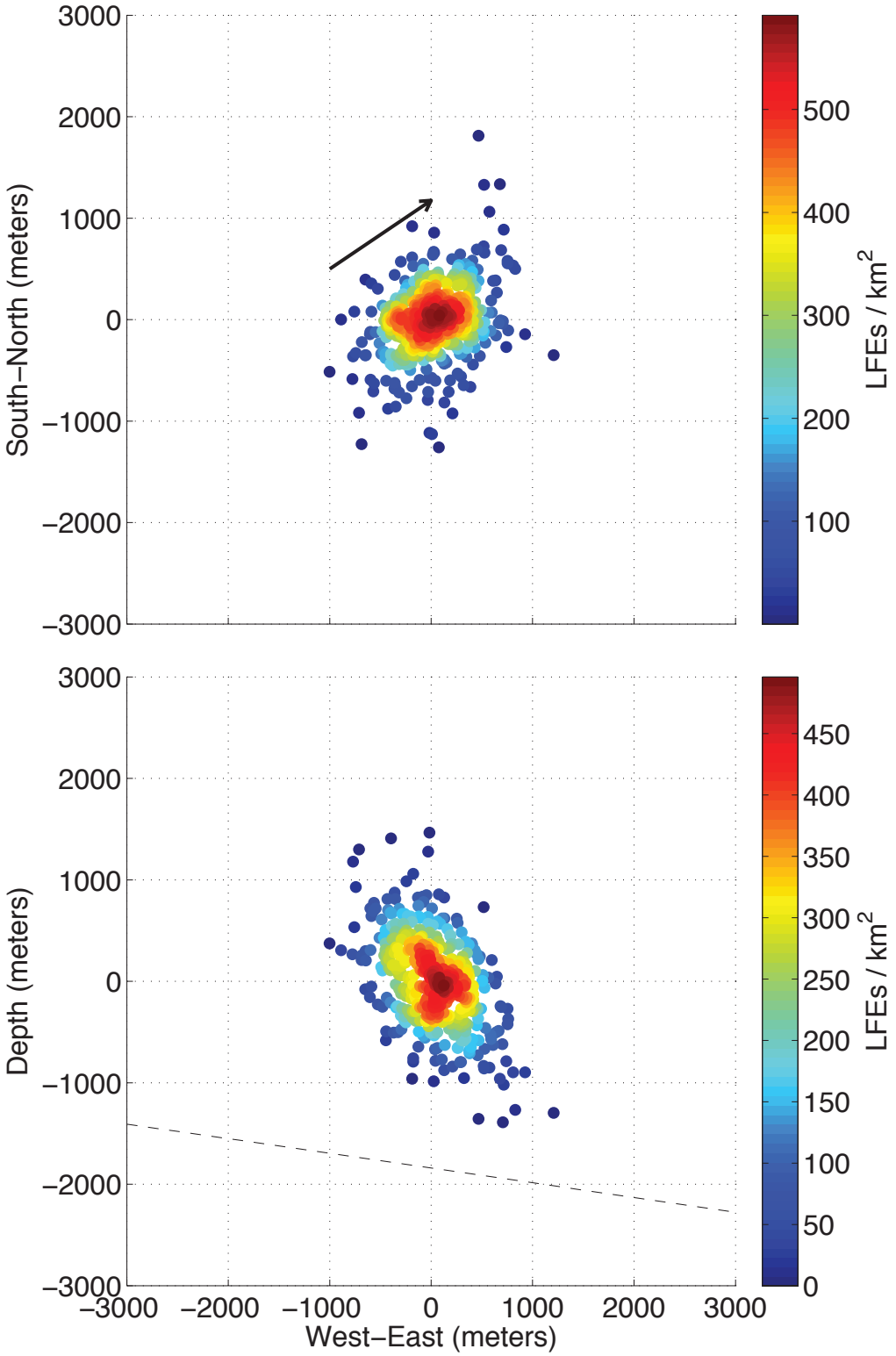

Figure 2.S4 – Map and cross section density plot of 431 LFE locations from LFE1. The plate convergence direction (black arrow) is shown in the top plot, and the *McCrory* (2012) (dashed line) plate interface model is shown in the lower plot.

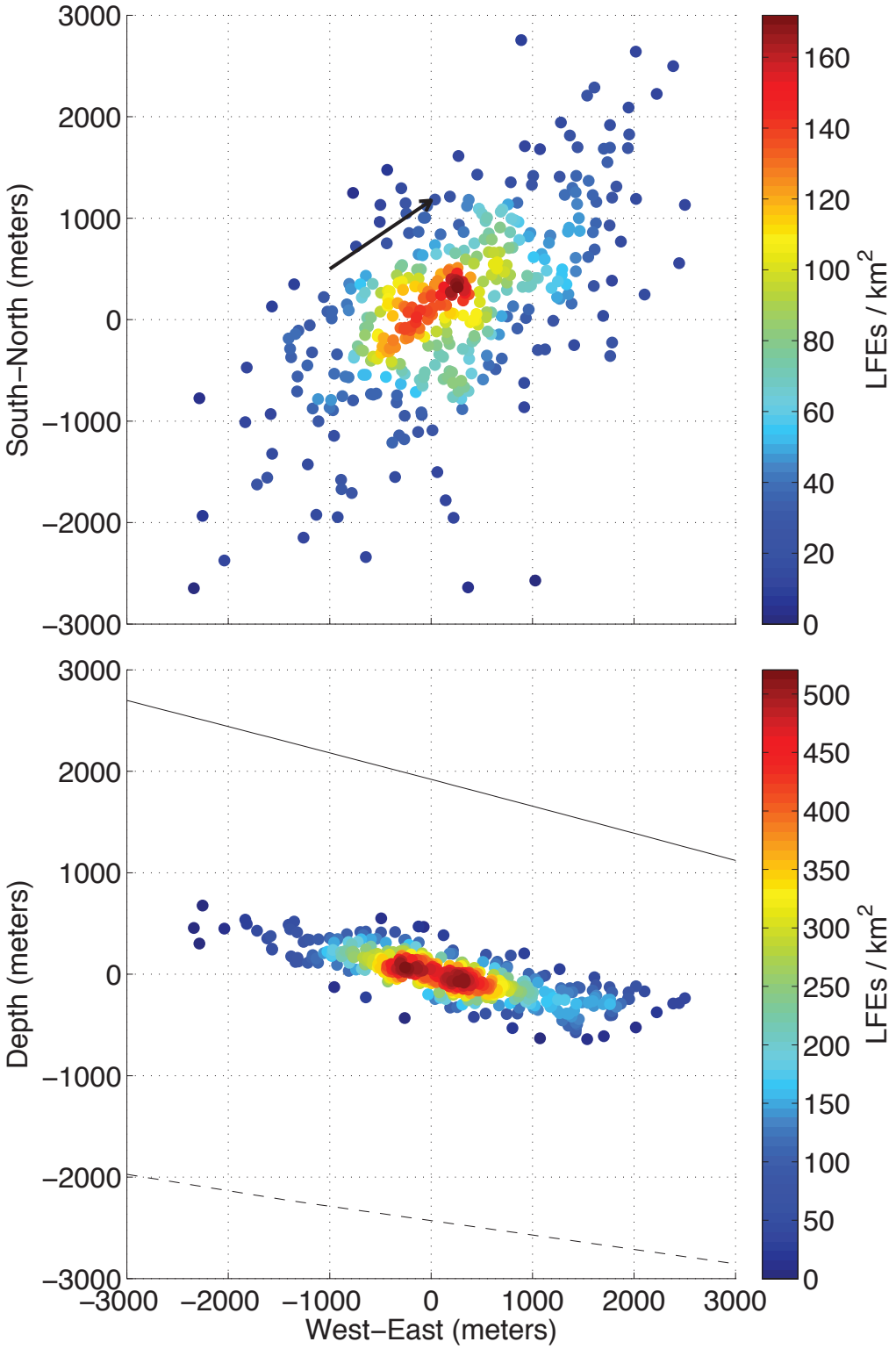

Figure 2.S5 – Map and cross section density plot of 405 LFE locations from LFE2. The plate convergence direction (black arrow) is shown in the top plot, and the *McCrory* (2012) (dashed), and *Preston* (2003) (solid line) plate interface models are shown in the lower plot.

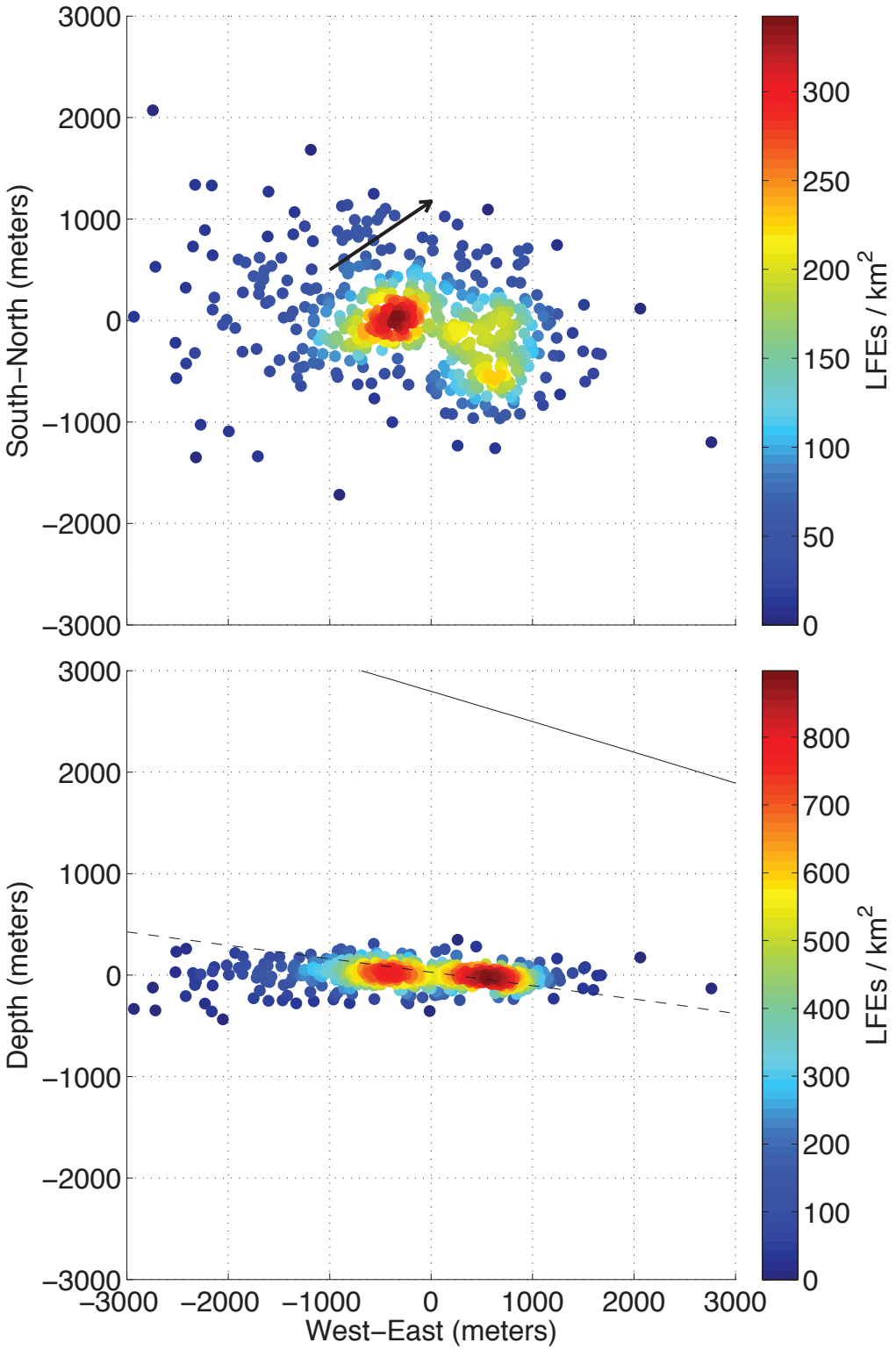

Figure 2.S6 – Map and cross section density plot of 533 LFE locations from LFE3. The plate convergence direction (black arrow) is shown in the top plot, and the *McCrory* (2012) (dashed), and *Preston* (2003) (solid line) plate interface models are shown in the lower plot.

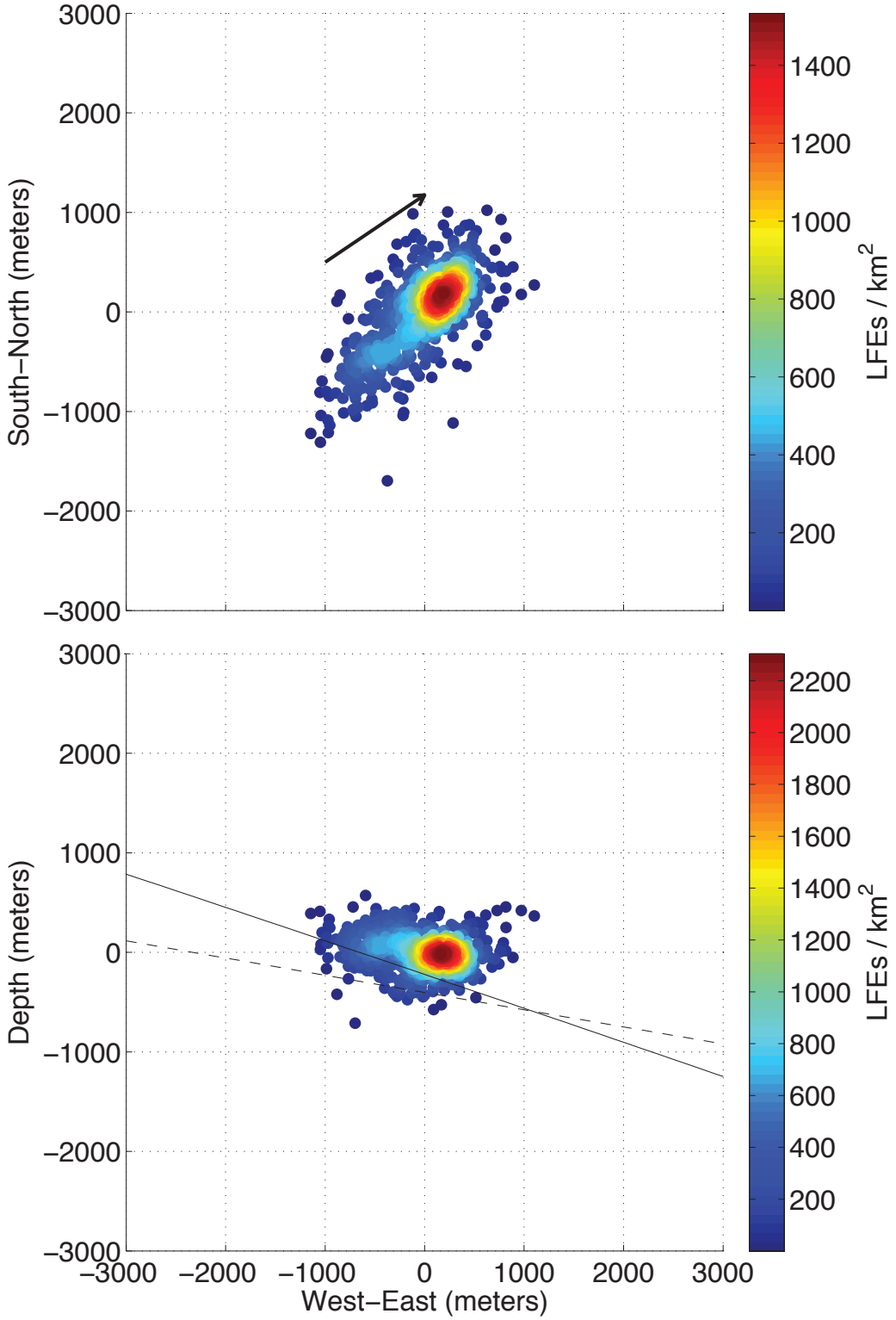

Figure 2.S7 – Map and cross section density plot of 758 LFE locations from LFE4. The plate convergence direction (black arrow) is shown in the top plot, and the *McCrory* (2012) (dashed), and *Preston* (2003) (solid line) plate interface models are shown in the lower plot.

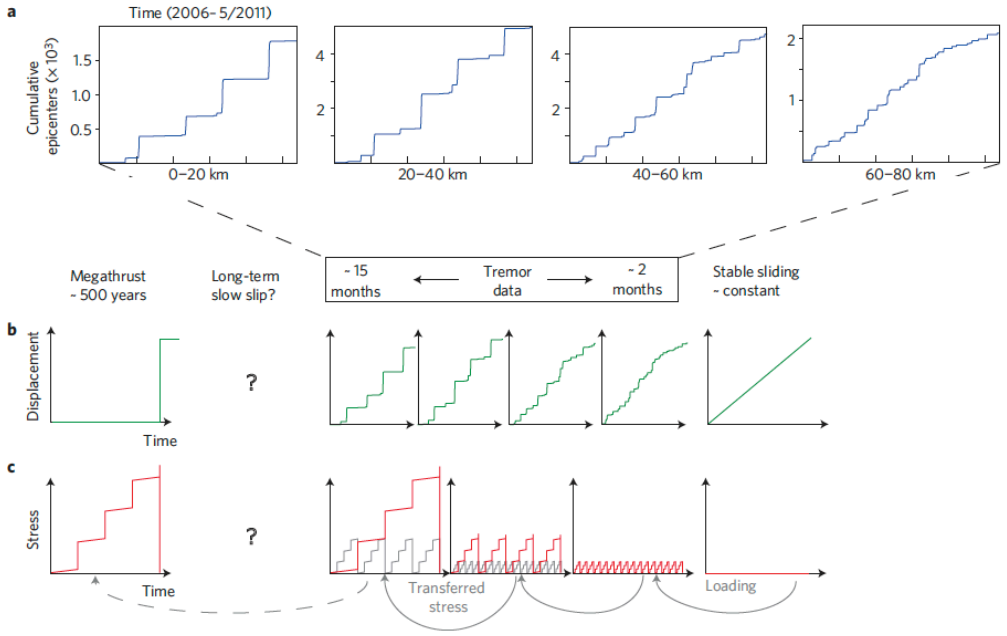

Figure 2.S8 – Figure from *Wech and Creager* [2011] showing their tremor swarm observations (a), which mirror what we see for our 4 LFE families (Figure 2.3). They propose a stress transfer model (c) that is loaded by stable creep downdip of the transition zone and transfers that stress updip in slow slip events of increasing size and duration governed by increasing friction updip.

Figure 2S.9 – Figure from *Kaproth and Marone* [2013] showing measured stress change (black lines) and displacement (grey lines) for 60 different episodes of slow slip. Note that different episodes have different amount of stress change and corresponding slip. The episode that most closely resembles what we see at LFE1 is around 25, where the grey curve shows a high initial rate of slip (what we see as LFE activity), transitioning to a slower rate with time (Figure 2.3).

III. A family of repeating low-frequency earthquakes at the downdip edge of tremor and slip

3.1 Introduction

Non-volcanic tremor—a low frequency, long duration seismic signal lacking distinct phase arrivals—was first identified in Japan [*Obara,* 2002] and has subsequently been found to correlate with deep slow slip on subduction zones in Cascadia [*Rogers and Dragert,* 2003] and Japan [*Obara et al.,* 2004]. Shortly thereafter, *Shelly et al.* [2007] demonstrated that tremor in Japan was at least in part composed of tiny, repeating low-frequency earthquakes (LFEs). Unlike tremor, LFEs often have distinct P and S phase arrivals—a characteristic that has been exploited to accurately locate the source of LFEs and associated tremor to very near the subduction interface in Japan [*Shelly et al.,* 2007], Cascadia, [*La Rocca et al.*, 2009; *Bostock et al.*, 2012], Costa Rica [*Brown et al.*, 2009], and also on the deep extension of the San Andreas Fault near Parkfield, CA [*Shelly et al.*, 2009]. The amplitude spectra of LFEs is deficient in high frequencies relative to similarly sized nearby earthquakes, but mirrors the spectra for tremor [*Kao et al.,* 2006; *Shelly et al.*, 2007]. LFE focal mechanisms in Japan [*Ide et al.*, 2007] and Cascadia [*Bostock et al.*, 2012] are in agreement with shallow thrusting in the direction expected for plate convergence, suggesting that LFEs represent small amounts of slip on the plate interface. We create and analyze a 5-year catalog of 9000 repeats of a single LFE family to examine the behavior of slow slip on the downdip extension of the Cascadia subduction zone beneath western Washington State. This LFE family is the deepest (most down-dip) and most frequently active family we have yet found. It lies on the far eastern edge of the region of PNSN tremor detections (2009-2013) [*Wech*, 2010] (Figure 3.1) and

at the down-dip edge of 122 LFE families in located in Northern Washington [*Royer and Bostock,* 2013]. Four of their LFE families were at similar depths, though not at the same location along strike as our LFE family. Their nearest LFE family is ~10km south of ours, and their next nearest is ~20km west. The frequency and regularity of our LFE family allowed us to quickly build up a large catalog of detections, making it a natural target for detailed analyses.

3.2 Method

We first identified this LFE through visual inspection of the data. We chose one of the highest signal-to-noise instances of this LFE and used that reference event to build up a template. A 15-second window containing the P- and S-waves for the reference event was auto-correlated with 12 hours of data for all available channels from the 1-km aperture Big Skidder (BS) array of six 3-component stations to find matching events. This array is part of the Cascadia Arrays For EarthScope (CAFE) experiment. The resulting fully normalized auto-correlation functions—one for each channel—were then combined using a third-root stack to identify time windows that correlated best across all 18 channels. Templates were built by linearly stacking the 80 best correlating windows, forcing identical time offsets for each station/channel. This process was repeated 3 times to further improve the quality of the templates. A complete catalog was then produced using a stack of fully-normalized running auto-correlations between each stacked template and its corresponding continuous 5-year long seismogram. For each day we calculate the median of the absolute deviation (MAD) of the stacked auto-correlation function. We chose to define a detection as a time when the stacked auto correlation

function exceeded 10*MAD, producing a typical threshold in which the mean correlation typically exceeded 0.2 to 0.3. Because the S minus P time is about 6 seconds, and there are often spurious detections when the P-wave of the template aligns with the S-wave of an LFE on the seismogram, we require the time between adjacent LFE detections to be greater than 6 seconds. The resulting catalog contains ~9600 detections. The vast majority of these are real, but a few percent appear to be erroneous, so we further filter these events as follows: 1) identify and remove events which occur within 30 seconds from the time of any nearby earthquakes in the Pacific Northwest Seismic Network (PNSN) catalog (~60 detections); 2) remove large amplitude events that occur during known periods of logging near our stations (~30 days in 2007); 3) remove isolated events that did not occur as part of larger LFE swarms and which were visually determined to be non-LFEs (~180 detections). Removing these false detections brought our final catalog size to 8942 events for the period October 2006 to September 2011. All events removed were inspected and either lacked P-waves, S-waves, or had an inconsistent S minus P time.

3.3 Temporal Distribution of LFEs: Time-Predictable Swarms

Our catalog of LFE detections is clustered into swarms of activity with <1% of events occurring outside of swarms. We define a swarm as at least 4 detections such that the largest gap between detections is less than 3 hours. By this metric our 5-year catalog is organized into 198 distinct swarms with 4 to 268 (median of 29) LFE detections per swarm, and ~150 isolated, non-swarm detections, most of which are clustered into groups of 2 or 3 LFEs, which may be small, signal-poor swarms. Swarms occur roughly every 8

to 9 days, although inter-swarm times are as short as 3 hours or as long as 4 weeks (Figure 3.S1). Dividing the total number of days in our LFE catalog by the total number of swarms yields an average recurrence interval of 8 days. We define swarm duration as the time between the 10^{th} percentile event and the 90^{th} percentile event. Swarm durations vary from 10 minutes to 12 hours, with a median duration of 1 hour.

Interestingly, we find that cumulative seismic moment for each swarm is positively correlated with the time until the next swarm (Figures 3.2 and 3.S2). Seismic moment for each LFE is estimated as described in section 5 below. The definition of swarms we use in this paper is somewhat arbitrary, so we consider 40 swarm catalogs defined by the minimum number of LFEs ranging from 4 to 12 and gaps of 3 to 24 hours between events. The mean correlation over this range of swarm definitions is 0.52 ± 0.03. These correlations are highly significant, with p-values ranging from 10^{-9} to 10^{-13}. These are the probabilities of achieving the observed correlations with random data. In contrast, comparing the cumulative swarm moment to the time since the last swarm for the same 40 catalogs produces correlations of 0.16 ± 0.03, with p-values ranging from 10^{-1} to 10^{-2}. Assuming that the fault stress is steadily increasing as a result of stable plate convergence down dip, our strong correlation with time until the next swarm can be explained by a model in which there is a constant stress threshold at which a swarm of LFEs will initiate. Once a swarm has begun, it will lower the state of stress on its portion of the fault by an amount proportional to the cumulative moment of the LFEs within that swarm. Given the cumulative swarm moment and assuming a constant rate of stress loading, one can predict the amount of time until the next swarm. In other words, swarms are time-predictable, not slip-predictable. This behavior contrasts with previously published slip-

predictable behavior of the deepest detected LFE family along the San Andreas Fault [*Shelly*, 2010].

3.4 Relative LFE Locations

To estimate the absolute location of our LFE family we cross-correlated stacked templates at different stations to measure differential S and P times between stations, and S minus P times at individual stations. Using data from the BS array and from three isolated stations with noise levels small enough to record these tiny LFEs, we employed a double-difference relocation method [*Waldhauser and Ellsworth*, 2000] to find precise relative locations for the 700 most highly correlating events from our catalog. Our data consisted of nearly 4 million auto-correlation-obtained differential times (1.4 million for P-waves, 2.6 million for S-waves) measuring the time between P waves (or S waves) for all event pairs on single channels. Compared to the starting solution that had all events at the same location, the relocated events resulted in a variance reduction of 73% (Figure 3.S3). In map view, the locations lie in a narrow patch elongated parallel to the plate convergence direction (Figure 3.3). The patch is approximately 2 km long and 500 m wide. Within this patch is a smaller, LFE-dense core that contains five times as many detections per square meter as the rest of the patch. The patch core is roughly circular with a radius of 300 m, and contains nearly half (46%) of the 700 relocated events. Individual LFE locations have formal errors of ~100 m, giving us confidence that the dimensions of our location cloud are real. The depth distribution of the locations is very small (<300 m), suggesting that the LFEs either lie on a plane or within a narrow volume. Additionally, LFE depths are within 1 km of two different plate interface models

[*Preston et al.,* 2003; *McCrory et al.*, 2012] and exhibit a similar dip angle to the east. This is consistent with nearby LFE locations from *Royer and Bostock* [2013]. The plate interface model of *Audet et al.* [2010] is about 5km shallower than the LFEs.

We also calculated double-difference relocations for the best correlating events within the 8 largest swarms. Among these swarms, we found 5 where locations migrated SW (up-dip), 2 where locations migrated NE (down-dip), and 2 where we found no evidence for systematic migration (Figures 3.S4-S6). Those swarms that did exhibit migration usually had speeds of ~1 km/hr. This observation recalls previously reported tremor streaks, also seen in Cascadia, which migrate rapidly up and downdip during ETS events [*Ghosh et al.*, 2010]. While tremor streaks usually travel tens of kilometers at speeds as high as 100 km/hr, our migrations are 50 to 100 times slower and only 1 to 2 km long. We postulate that a migrating pulse of slow-slip is responsible for producing the LFE migrations we observe. This slow-slip pulse likely extends over an area larger than our LFE patch; however, the lack of any LFEs and/or significant tectonic tremor within 10 km of this family prevents any direct observations to measure the size of the slow-slip pulse.

3.5 LFE Amplitudes and Seismic Moment

To determine LFE amplitudes, we measured the peak-to-peak S-wave amplitude on horizontal channels at six 3-component stations within the 1 km-aperture BS array. All stations had instrument responses deconvolved to displacement, and were bandpass filtered from 2 to 8 Hz. The amplitude assigned to each LFE was the median peak-to-peak amplitude from the stations used for that event. To ensure accuracy, for each LFE

we only kept channels where the time of the peak amplitude matched to within 0.2 s of each other. Out of 12 total horizontal channels available, all channels were kept and used for 70% of the LFEs. We found a narrow range of LFE amplitudes that spanned from 0.2 to 18 nm. Amplitudes measured by the same method on velocity seismograms are up to one order of magnitude larger than LFE amplitudes reported on the San Andreas Fault (SAF) [*Shelly and Hardebeck*, 2010] despite the fact that our source-receiver distance is greater.

In order to better understand the physical characteristics of the LFE sources we convert LFE amplitudes to seismic moment. This proved trickier than we had anticipated, primarily because high noise levels in the displacement spectra made it difficult to measure spectral values below the LFE corner frequencies. Instead we use nearby small earthquakes to convert LFE amplitude to local magnitude (M_L) and then convert local magnitude to seismic moment.

To convert LFE amplitudes to M_L we found eight nearby intraslab earthquakes that were also in the Pacific Northwest Seismic Network (PNSN) catalog with assigned local magnitudes. Seven of the events were located at similar depths and within 10 km of the LFEs and had M_L values between 1.2 and 1.6. The other event was a larger 4.5 magnitude earthquake that was about 17 km below the location of the LFEs. We measured median peak-to-peak S-wave amplitudes for the earthquakes in the same way and at the same stations as for the LFEs. The local magnitude is based on the displacement amplitude measure on a standard Wood-Anderson seismometer, which is unusual in the sense that its response is flat to displacement at high frequencies. M_L is defined as:

$$M_L = \log_{10} A + c_1 \quad (3.1)$$

where A is the measured peak amplitude and c_1 is a correction for distance [*Shearer*, 1999]. We determine the value of c_1 for the seven small earthquakes that are all the same distance from the stations as the LFEs. For peak-to-peak amplitude A measured in meters, the earthquake-determined correction factor c_1 is 8.65 ± 0.4.

Next, we follow the method of *Shearer et al.,* [2006] who analyzed tens of thousands of small earthquakes in California comparing catalog local magnitude values against estimates of relative seismic moment made from low-frequency spectral-amplitude measurements and found that:

$$M_L = 0.96 \log_{10} M_0 + c_2 \quad (3.2)$$

where M_0 is the seismic moment in Newton-meters. The factor 0.96 is a robust and important result of their paper and is surprising because for moment magnitude (M_w) this factor is 0.667. The constant c_2 is determined by using the standard relationship between M_w and M_0 [*Hanks and Kanamori*, 1979] and assuming that M_L is equal to M_w at magnitude 3 [e.g. *Shearer et al.*, 2006]. This assumption is significant in that it determines the overall estimated moment of all the LFEs.

By combining equations (3.1) and (3.2) and rearranging terms we arrive at an expression for converting our measured LFE amplitude $A(m)$ to seismic moment (N-m):

$$M_0 = 10^{(c_1 - c_2)1.04} A^{1.04} = 2.7 \times 10^{19} A^{1.04} \quad (3.3)$$

Thus we used PNSN catalog local magnitudes to translate our observed LFE amplitudes to local magnitudes and then scaled these to seismic moment. It should be noted that due to the uncertainty in the scaling between measured LFE amplitudes and M_L, as well as between M_L and M_w, our absolute moment values are approximate and are not as well constrained as the relative moments among the events. Our calibration to M_L using 7

small earthquakes has a magnitude uncertainty of ±0.4 and the scaling from M_L to M_w would change by 0.33 if the assumed cross over point changed by 1 unit of magnitude. Resulting LFE moments range from 2.9×10^9 N-m (M_w0.3) to 2.3×10^{11} N-m (M_w1.5). Moment magnitudes less than 1 show significant day/night variation in detection levels, suggesting that our catalog is complete above this level but incomplete below it (Figure 3.S7).

The number of LFEs bigger than a given amplitude is better explained by an exponential distribution than by a power-law distribution (Figure 3.4). Two previous studies of tremor and LFE amplitudes have also reported exponential amplitude distributions [*Watanabe et al.*, 2007; *Shelly and Hardebeck,* 2010]. Fitting a line through the power-law distribution for the largest 1000 LFEs would produce a b-value (slope) of about 4, meaning that there are many more small events for a given number of big events than seen for regular earthquakes, which have b-values near 1. However, the slope varies continuously at smaller amplitudes suggesting this is not the appropriate distribution. The exponential distribution can be described as:

$$\boldsymbol{N = c_3\ 10^{-A/A_0}} \qquad \textbf{(3.4)}$$

where N is the number of LFEs with amplitude bigger than A, $A_0 \sim 4.5$ nm, and c_3, the total number of LFEs, is about 10^4. The average amplitude in this distribution is $log_{10}e \times A_0 = 2$ nm. The number of events falls off by a factor of 10 for every increase in amplitude of A_0. According to our calibration equation (3.3) this increase corresponds to M_w1.1, or $M_0 = 5.6\times10^{10}$ N-m.

3.6 Discussion

Major Episodic Tremor and Slip (ETS) events occur regularly in this part of Cascadia [*Rogers and Dragert*, 2003; *Wech et al.*, 2009], and appear to trigger activity at our LFE family, although very few tremors are observed this far downdip during ETS. During each of the five ETS events between 2007 and 2011 in northern Washington we detect LFE activity within 1 to 3 days following vigorous updip tremor activity. In four of the five cases LFE swarms occurred. However, since swarms recur every 8 days or so, it is difficult to be definitive. Additionally, the LFE swarms observed during ETS are not systematically bigger or different than the other 50 swarms that occur over the course of each ETS cycle. We interpret the activity of this family as primarily a result of smaller but more frequent episodes of slow-slip at and around the location of this LFE [e.g. *Wech and Creager*, 2011]. These small, frequent slips are likely driven by continuous slow-slip just downdip of this LFE at the junction between the assumed constantly-creeping zone and the tremor/LFE zone. Interestingly, we find no other detectable LFEs within 10 km of this LFE family. The isolation of this LFE family is unique, and allows us to examine detailed LFE behavior without contamination from other nearby families, as occurs in the more LFE-dense ETS zone updip.

The northeast-southwest trend of the LFE hypocenters suggests that the LFE locations are influenced by the plate convergence direction. In addition, the highest density of locations appears to be located on the downdip (northeastern) end of the distribution, which strongly suggests that the feature responsible for creating these LFEs resides on the down-going Juan de Fuca (JdF) plate. In this view, the locations updip of the high-density spot can be seen as a wake of LFEs following behind the primary

location of LFE generation. One possible explanation for this arrangement is the presence of a seamount, or other locally unique geologic formation on the JdF plate that is able to radiate seismically in LFEs when slipping while the adjacent areas around it are not. The fact that the distribution of LFE locations is also very thin vertically, and dips towards the east at depths coincident with several plate models is consistent with these LFEs locating on the plate interface. The vertical spread is ~300 meters, which could indicate the thickness of the region responsible for slow slip, but given uncertainties in relative LFE locations, the slow slip could also be confined to a much thinner fault. At any rate it is not likely to be broader than 300 m.

The finding that nearly all the LFEs occur as part of swarms, rather than isolated events, suggests that the LFEs are being externally driven, likely by small, frequent pulses of slow-slip. This idea is further supported by the observed migration trends in the double-difference locations for this LFE family, which often show systematic progression updip or downdip (Figures 3.S4-S6). The frequency of swarms indicates that small slow-slip events at this location occur 50 times more often than the larger ETS events seen in this part of Cascadia [*Rogers and Dragert*, 2003]. If the LFEs were occurring independently, rather than being externally driven, one would expect them to occur with a more random distribution in time.

We find that the median amplitude of individual LFEs increases during a swarm by about 30% (Figures 3.5 and 3.S8). This suggests that in order for all or most of the patch to rupture in a single event (and thus produce a large LFE) the patch might first need to be "unlocked" by smaller ruptures from smaller LFEs prior to the full rupture. The increase in amplitude may also result from stronger coupling in the patch core. A

plot of the 50 largest LFEs from the 700 relocated events supports this idea by showing that most of these large LFEs are located on or near the patch core (Figure 3.3, left side). In contrast, a plot of the 50 smallest LFEs from this same set shows that they are scattered throughout the larger LFE patch (Figure 3.S9). It should be noted that the location uncertainties for the smallest 50 LFEs are not significantly larger than those for the 50 largest LFEs. The largest LFE we detect during our 5-year dataset is about M_w1.5, which suggests that the patch dimensions do not permit larger events to occur at this location. Rubin and Armbruster [*2013*] found a similar pattern of increasing amplitudes during LFE swarms beneath southern Vancouver Island, though the LFEs they analyzed were farther updip than ours.

We use two approaches to estimate the size of the patch responsible for generating LFEs. The first approach relies on the distribution of the double-difference event locations. This distribution shows that a small area (radius ~300 m) contains the highest density of LFE locations. This same area also contains nearly all of the largest individual LFEs, as well as half the total moment of the entire LFE family. For these reasons we use 300 m as one estimate of the size of the LFE patch. Our second approach relies on our estimate of the total LFE moment, as well as the plate convergence rate to derive the expected patch size. For this approach, we assume that at the location of the LFEs the plate interface is not accumulating any stress over the 5-year period of our catalog. This implies that the amount of slip at the location of the LFEs should be equal to the slip predicted by the plate convergence rate over the same period. This is supported by the observation that the LFE moment rate does not change during our 5-year observation period. The total moment of all the LFEs in our 5-year catalog is

2.6×10^{14} N-m (M_w3.6), which is almost certainly an underestimate of the true moment release for two primary reasons. Firstly, our catalog only keeps events separated by more than 6 seconds, which would fail to include even large amplitude LFEs that often occur in rapid succession. Secondly, based on the differing rates of detection seen for events smaller than M_w1 during the day vs. during the night, our catalog is missing some of these smaller events during noisy periods. Despite these limitations, we make use of our 5-year total moment, along with the predicted slip over the same period provided by the plate convergence rate (~40 mm/yr) [*McCaffrey et al.*, 2007] to estimate the average patch size responsible for the LFEs we observe. Seismic moment is defined as:

$$\boldsymbol{M_0 = \mu D A} \qquad \textbf{(3.5)}$$

where μ is the shear modulus, D is the amount of slip, and A is the area that slipped. We use $\mu = 3\times10^{10}$ N/m^2 which splits the difference between that expected for typical subducted oceanic crust at the appropriate depths (4×10^{10}) and values consistent with a highly anomalous upper oceanic crust with V_p/V_s ratios of order 2.4 [*Audet et al.*, 2009]. If the plate interface is divided into regions that only slip seismically—producing LFEs—and regions that slip totally aseismically, then the LFE generating area, determined from (3.5) using cumulative seismic moment and total plate-rate slip, is limited to a circle of radius 100 m. Alternatively, the LFE generating patch could sometimes slip seismically and sometimes aseismically.

In order to better understand which parts of the patch are most efficient at radiating LFEs, we estimate the LFE locking efficiency. Similar to seismic efficiency, we define the LFE locking efficiency as the proportion of the total slip that is accommodated by detected LFEs. We sum the individual moments of the 700 relocated

LFEs using a Gaussian smoothing scheme that distributes the moment of each LFE over a Gaussian distribution with a half width of 25 m. This produces a map of total moment per square meter. Using equation (5) and dividing by μ delivers a map of total slip during 5 years. Assuming the actual slip on the plate interface is equal to the plate rate over the time period of our catalog, we divide our total slip by the amount predicted by plate rate to obtain LFE locking efficiency. The highest LFE locking efficiency occurs in two small (~50 m radius) areas and reaches only about 20% (Figure 3.3, right side). These small high-efficiency areas both fall within a larger area of elevated locking efficiency that is bounded by our 300 m radius patch core. Due to uncertainties, it is possible that most of the slip expressed as observed LFEs occurs within these two small high efficiency areas. As mentioned previously, it is likely that the total moment we observe is less than the true moment. This could explain why the LFE locking efficiency never approaches 100%. It is likely, however, that some or most of the moment is expressed aseismically—even within our patch core.

Finally, we make use of estimates of patch size and moment to calculate the stress drop associated with a single LFE. Using the exponential distribution seen in our amplitude catalog, we select an LFE of characteristic size (M_w1.1). The stress drops for a circular fault with moment magnitude 1.1 and radii of 100 and 300 meters are 20 and 1 kPa, respectively [*Brune*, 1970] (Figure 3.S10). These values are several orders of magnitude less than the stress drops typical for similarly sized ordinary earthquakes. If, on the other hand, we assume each LFE in a swarm ruptures only a portion of the larger patch, then the fault radius for an individual LFE could be <<100 m, yielding stress drops on the order of 10^5 or 10^6 Pa, which would be similar in size to those seen in ordinary

earthquakes. It should be noted that if LFEs do have stress drops close to those of ordinary earthquakes that would not imply that LFEs and ordinary earthquakes are in other ways similar. A small stress drop makes sense given the fluid-rich, high pore pressure environment thought to exist near the plate interface in regions with detectable tremor and LFEs [*Shelly et al*., 2006]. In fact, tidal stresses of order 1 kPa as well as stress from surface waves of large teleseismic earthquakes have been observed to strongly modulate tremor in Cascadia and elsewhere [*Rubinstein et al.*, 2007, 2008; *Gomberg et al.,* 2008].

3.7 Conclusions

In summary, the isolated LFE family we examined revealed a number of interesting characteristics. LFEs in this family are clustered into swarms occurring on average every week. Cumulative LFE seismic moment for each swarm correlates strongly with the time until the next swarm, suggesting that these LFE swarms are time-predictable. Double-difference locations for 700 members of this family show a pattern of locations elongated parallel to the plate convergence direction. These locations dip eastward and occupy a narrow plane <300 m thick that lies very near the location of two different plate interface models. Peak-to-peak LFE amplitudes range from 0.2 to 18 nm and correspond with moment magnitudes of 0.3 to 1.5. LFE amplitudes are observed to increase during swarms, with the largest events usually occurring at the end of swarms. Nearly all of the largest events locate within a 300 m radius patch core coincident with the region of highest LFE location density. We propose a model where smaller LFEs in the early part of a swarm may serve to unlock the patch core and allow it to fail at the end

of the swarm in the form of a high amplitude LFE. LFE locking efficiency indicates that a maximum of 20% of plate rate slip is accommodated by LFEs, and only in two small patches (~50 m radius) within the larger patch core. Depending on assumptions, we estimate stress drops of only a few kilopascals or as high as several megapascals during individual LFEs at this location.

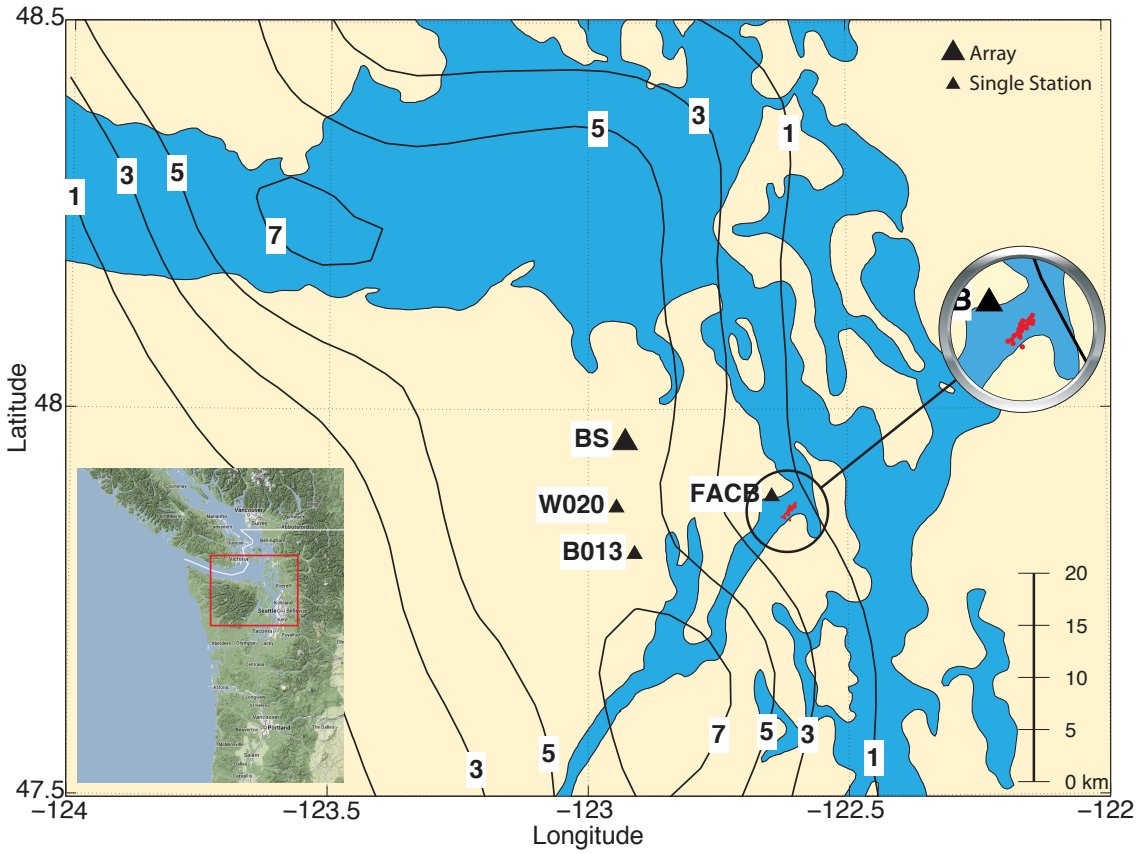

Figure 3.1 – Map showing LFE locations (red dots), contours of 2009-2013 tremor density per square kilometer [*Wech*, 2010] and stations used in double-difference relocation of LFEs (triangles). There are 6 stations in the BS array.

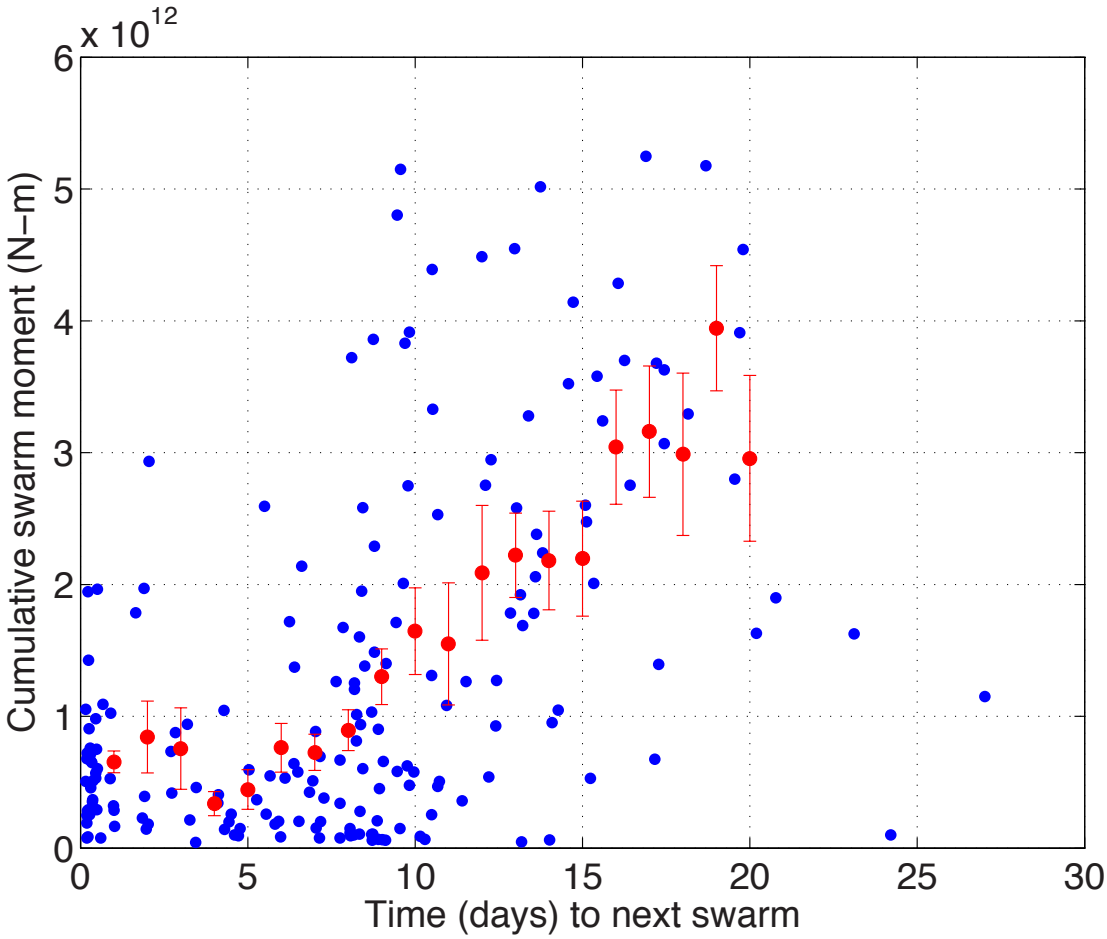

Figure 3.2 – Cumulative swarm seismic moment versus the time (days) until the start of the next swarm for our 198-swarm catalog. The statistically significant correlation (0.51) suggests that swarms are time-predictable. Increasing the minimum number of LFEs and the minimum gap between LFEs per swarm produces swarm catalogs that reduce the number of swarms clustered near the x and y axes and further improves the correlations (e.g. Figure 3.S2a). Dots with error bars indicate mean and standard deviation of the mean for 1-day bins that contain at least 4 observations.

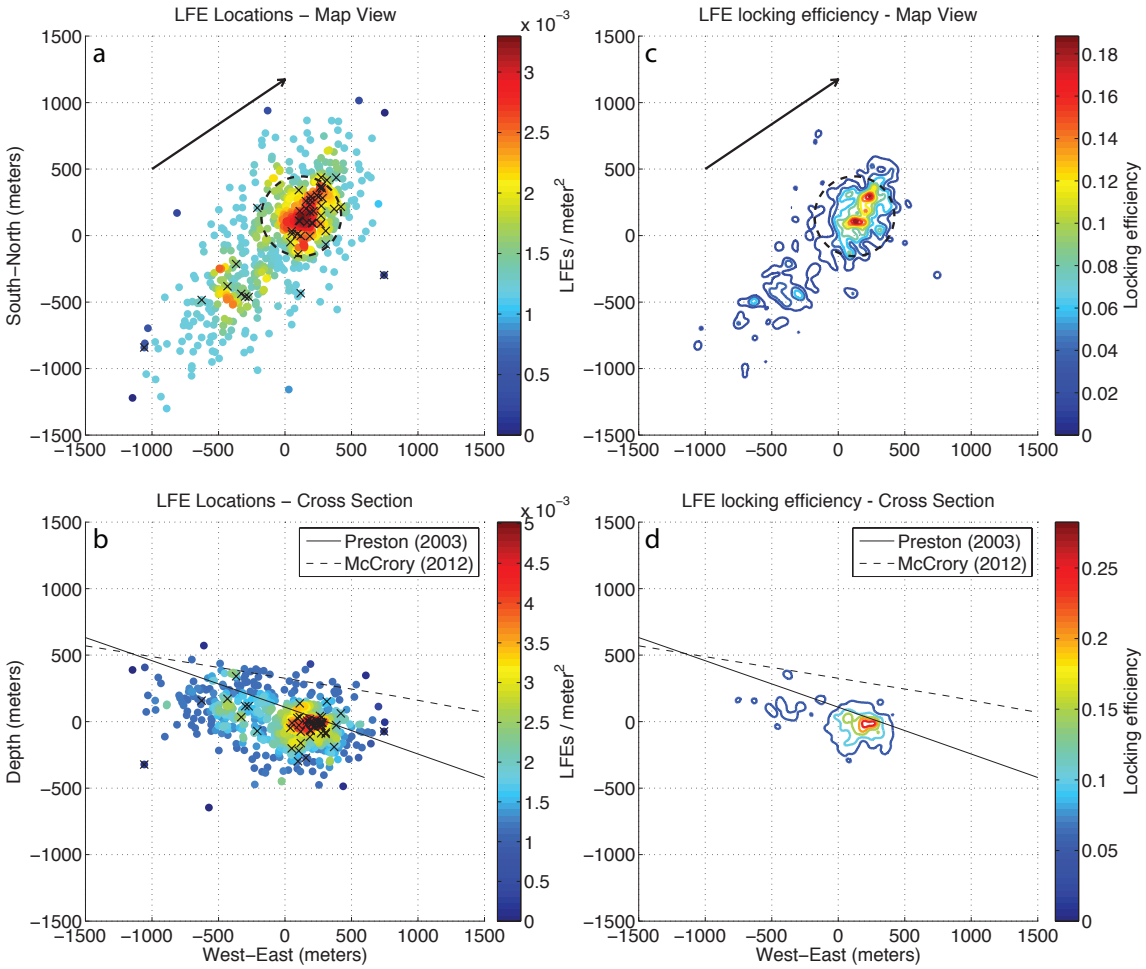

Figure 3.3 – Locations of 700 relocated LFEs colored by density in map view (a) and cross section (b). LFE locking efficiency (c, d) for same set of LFEs contoured at 0.05 intervals. Nearly half the LFEs lie within a 300 m radius of the patch core (dashed circle, a and c). The largest 50 LFEs (black crosses, a and b) cluster near the patch core. LFE distribution is elongated in the direction of plate motion (black arrow, a and c) and occurs near the depths of plate interface models from *Preston et al.*, [2003] (solid line, b and d) and *McCrory et al.*, [2012] (dashed line, b and d).

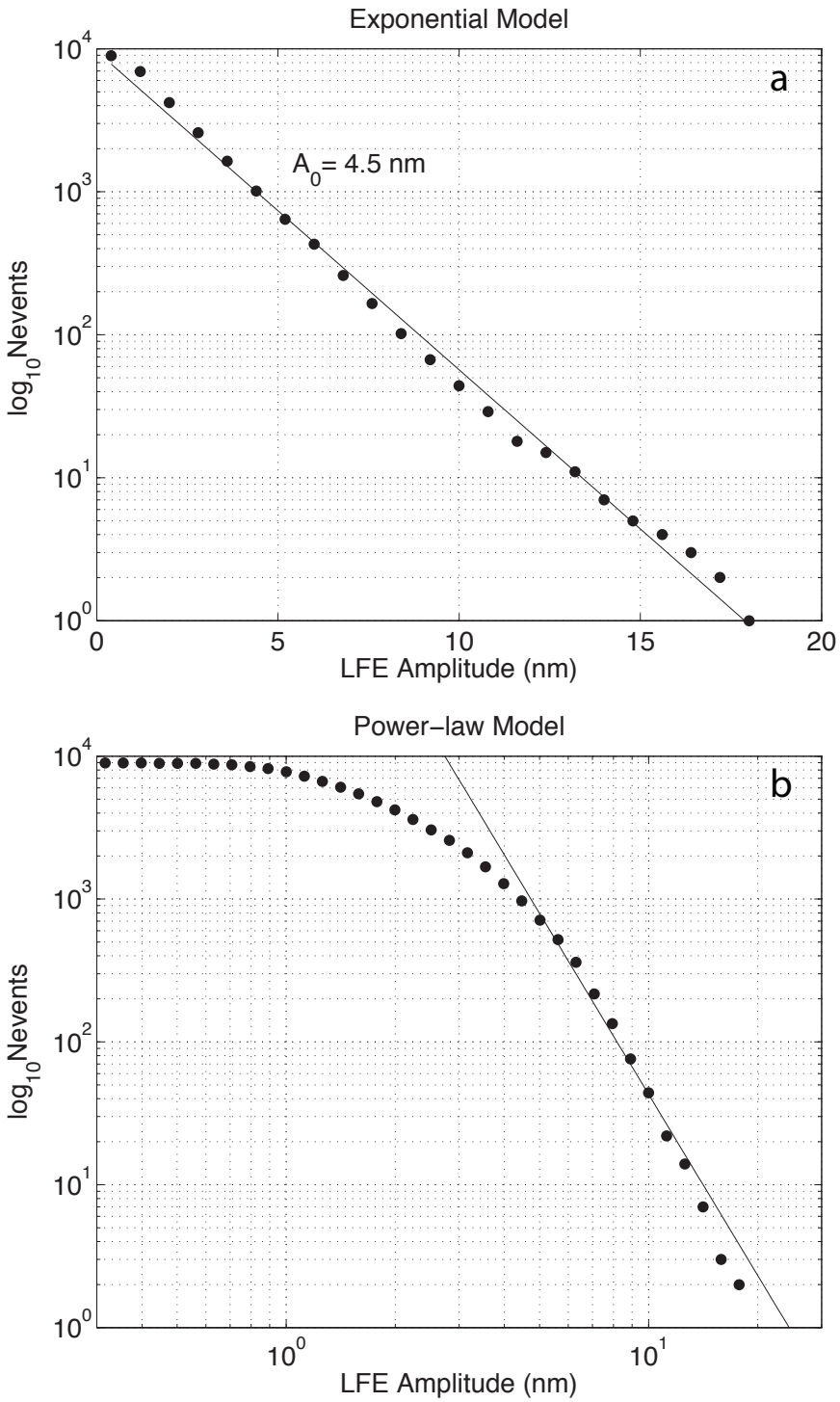

Figure 3.4 – Log-linear (a) and log-log (b) plots of number of LFEs above a given amplitude. An exponential distribution (a) fits the observations best with characteristic amplitude of A_0 = 4.5 nm where $N = N_0 \times 10^{-A/Ao}$. The Power-law Model (b) is most consistent with a very large b-value of 4.2 (black line).

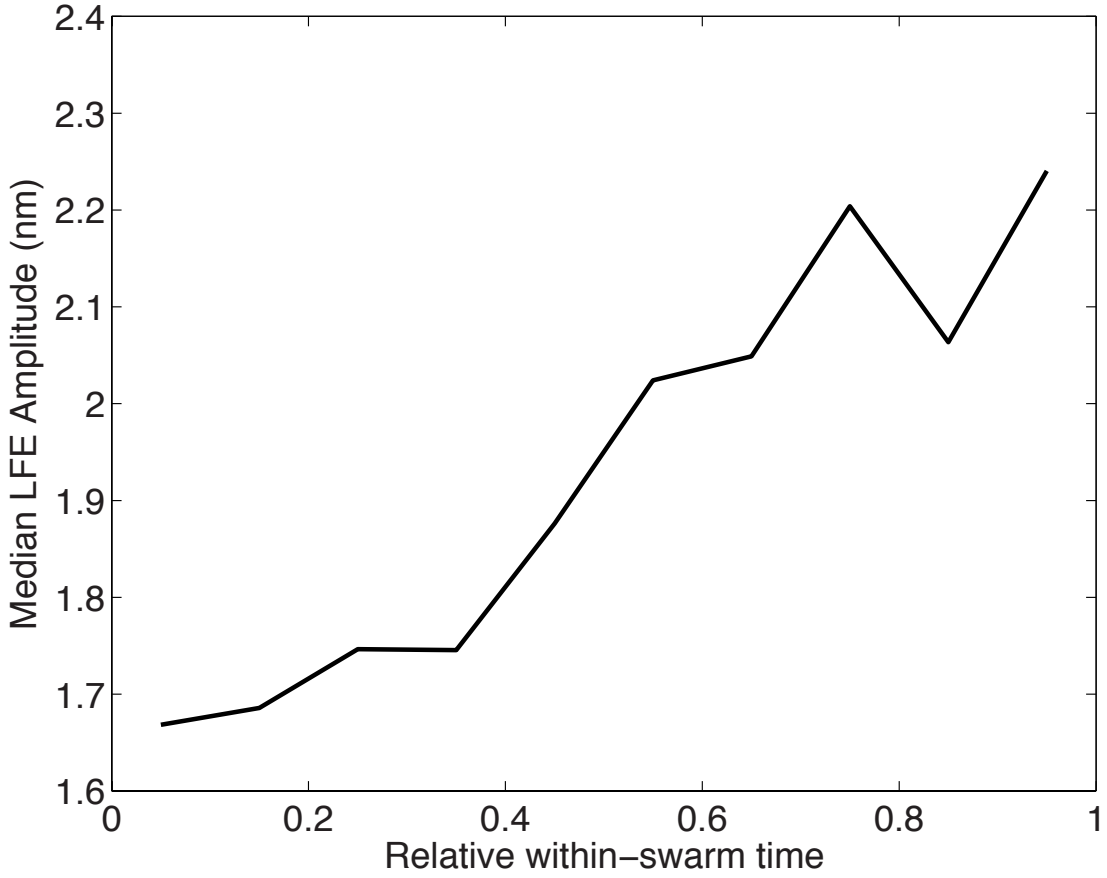

Figure 3.5 - Individual LFEs are binned by the relative within-swarm time of their occurrence showing the median displacement amplitude. The median LFE amplitude increases systematically from the beginning to the end of a swarm—suggesting smaller events may first be needed to unlock the patch core for failure in larger events towards the end of the swarm.

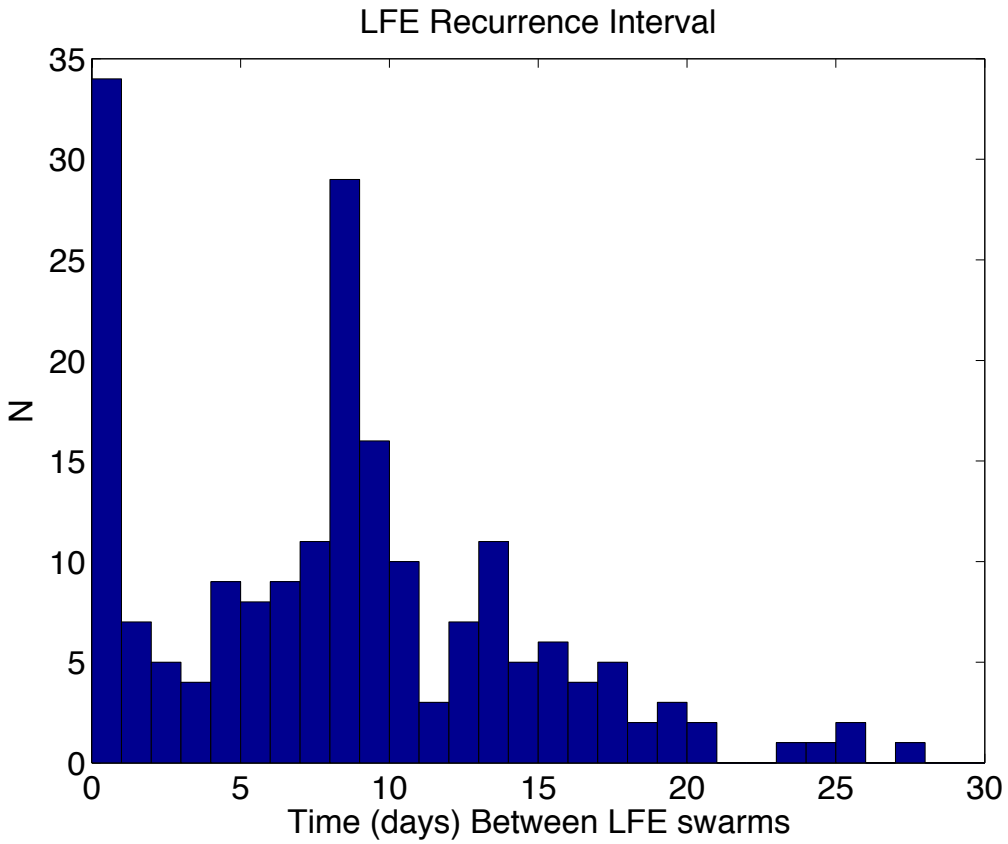

Figure 3.S1 – Histogram of the time (days) between each of the 198 LFE swarms in our catalog. The large peak near 0 days is indicative of the fact that in the immediate aftermath of a swarm, there is a high likelihood for additional follow-on swarms to occur. It could also be an artifact of our swarm definition that groups events into different swarms if there is a gap of 3 or more hours between event detections. Increasing this gap allowance consolidates many of these short-recurrence swarms into larger swarms. The peak near 8 days coincides with the average recurrence interval. Later peaks near 16 and 24 days could result if we fail to capture a weak swarm or two, and thus have a recurrence interval 2 or 3 times as long.

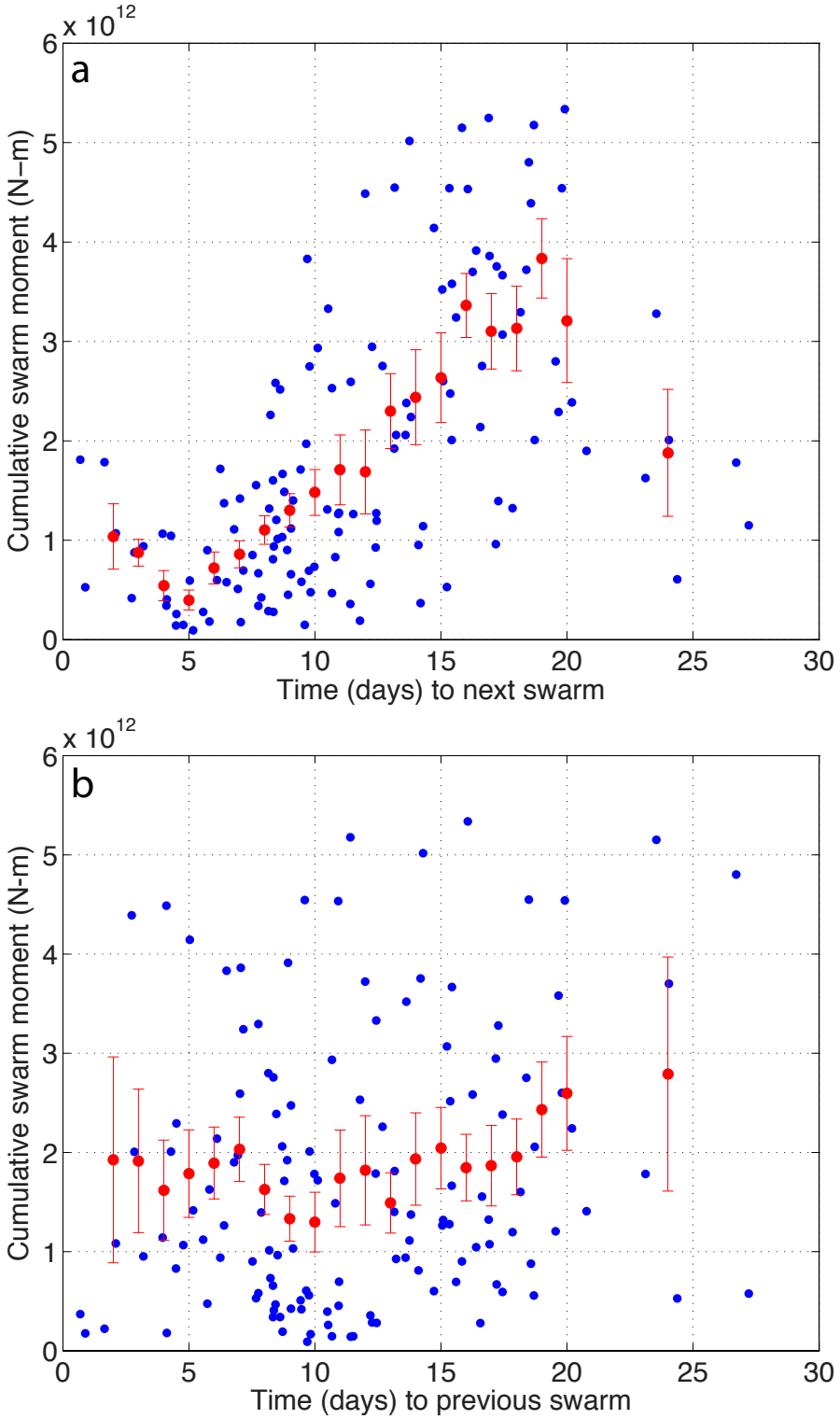

Figure 3.S2 – Cumulative swarm moment versus (a) the time (days) until the start of the next swarm, and (b) the time (days) to the previous swarm for swarms with at least 10 LFEs and no gaps greater than 9 hours between LFEs. The statistically significant correlation (0.54) seen in (a) and the lower correlation (0.19) seen in (b), suggests that swarms are time predictable and not slip predictable.

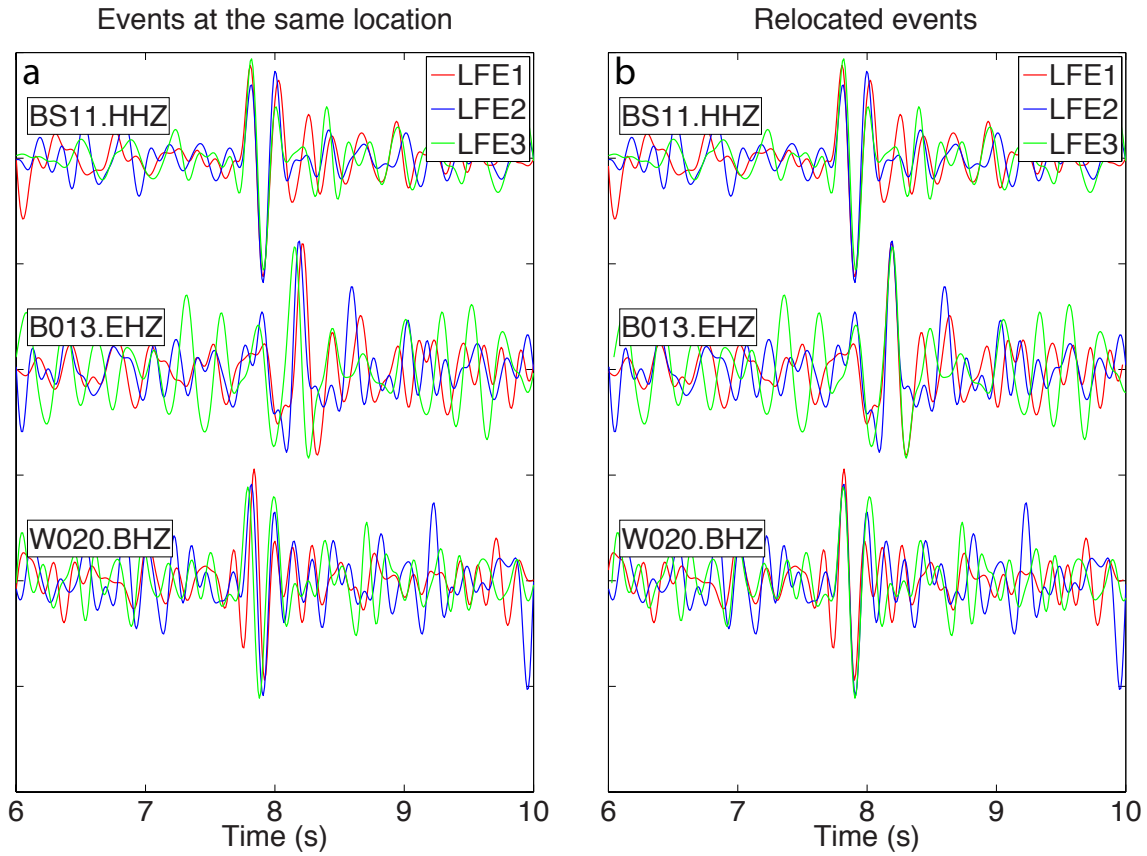

Figure 3.S3 – Comparison of three relocated LFEs as observed before and after relocation at three different stations. Left plot (a) shows P-waveform alignment if each of the three LFEs is forced to be at the same location. Right plot (b) shows waveform alignment if the LFEs are at their relocated positions. We chose LFE1 from the northeast (downdip) end, LFE2 from the center, and LFE3 from the southwest (updip) end of the location cloud. The distance between LFE1 and LFE3 is 1.5km. The better fit seen in the right plot gives us confidence that the size and orientation of our relocated LFE cloud is accurate.

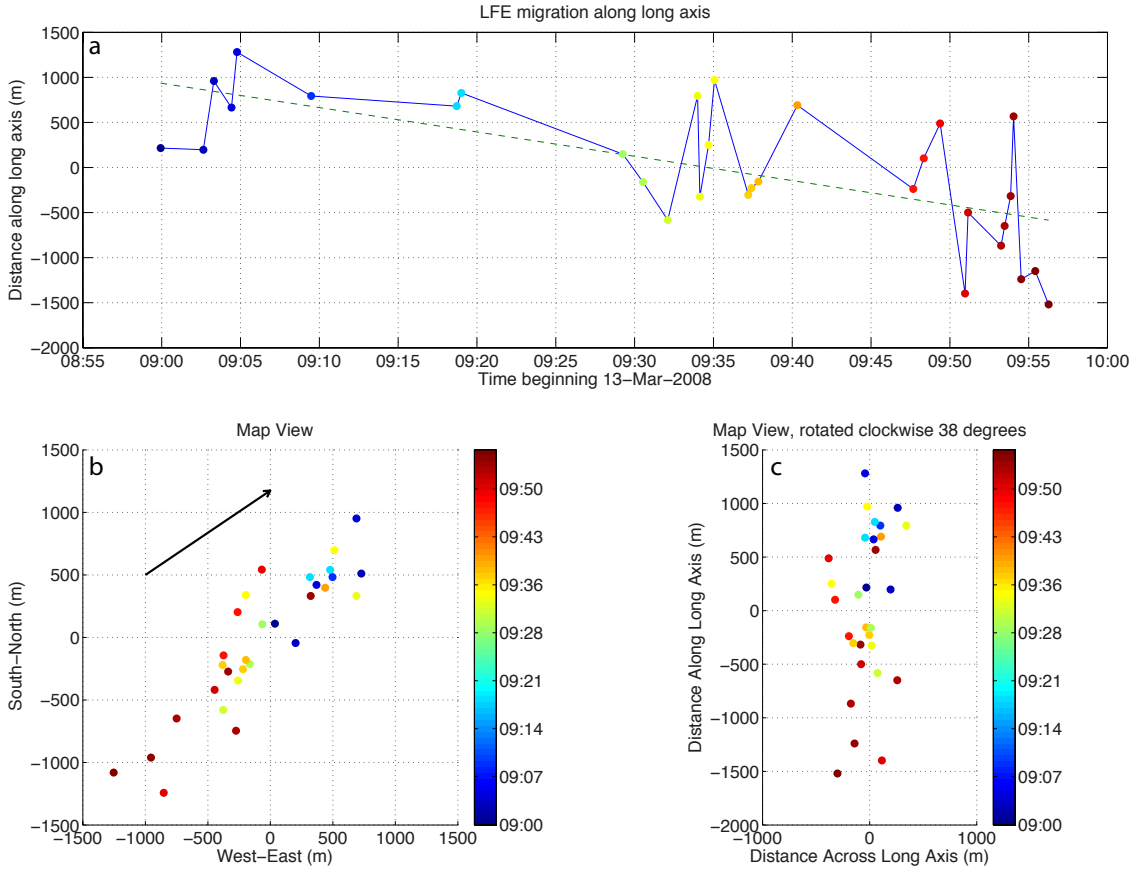

Figure 3.S4 – Example of updip migration seen in a single LFE swarm. The overall migration along the long axis of the swarm is plotted vs. time (a), and is shown in map view (b), as well as in a map view that is rotated clockwise 38° from north (c). Average migration velocity is 1.5 km/hr (a, dashed green line).

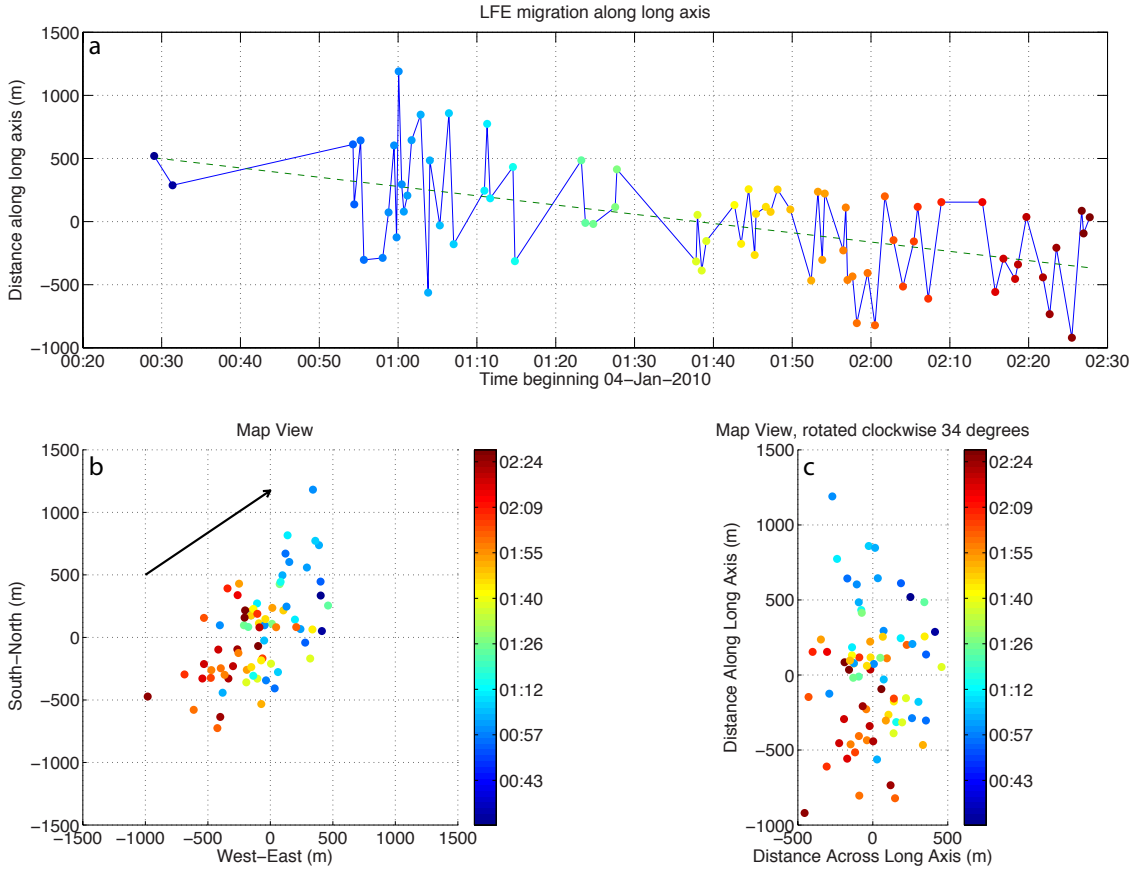

Figure 3.S5 – Example of updip migration seen in a single LFE swarm. The overall migration along the long axis of the swarm is plotted vs. time (a), and is shown in map view (b), as well as in a map view that is rotated clockwise 34° from north (c). Average migration velocity is 0.4 km/hr (a, dashed green line).

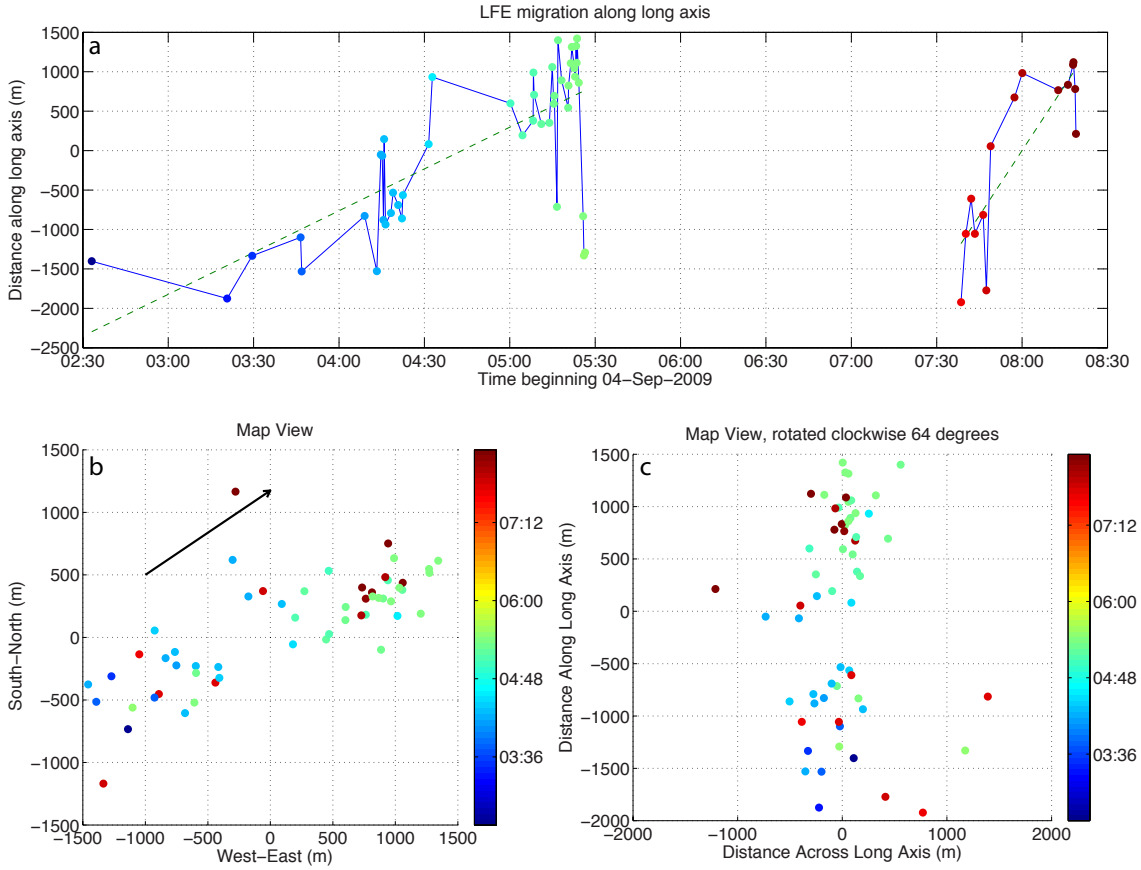

Figure 3.S6 – Example of downdip migration seen in 2 LFE swarms. The overall migration along the long axis of the swarm is plotted vs. time (a), and is shown in map view (b), as well as in a map view that is rotated clockwise 64° from north (c). Average migration velocity is 1 km/hr for the earlier swarm and 2.7 km/hr for the later swarm (a, dashed green lines).

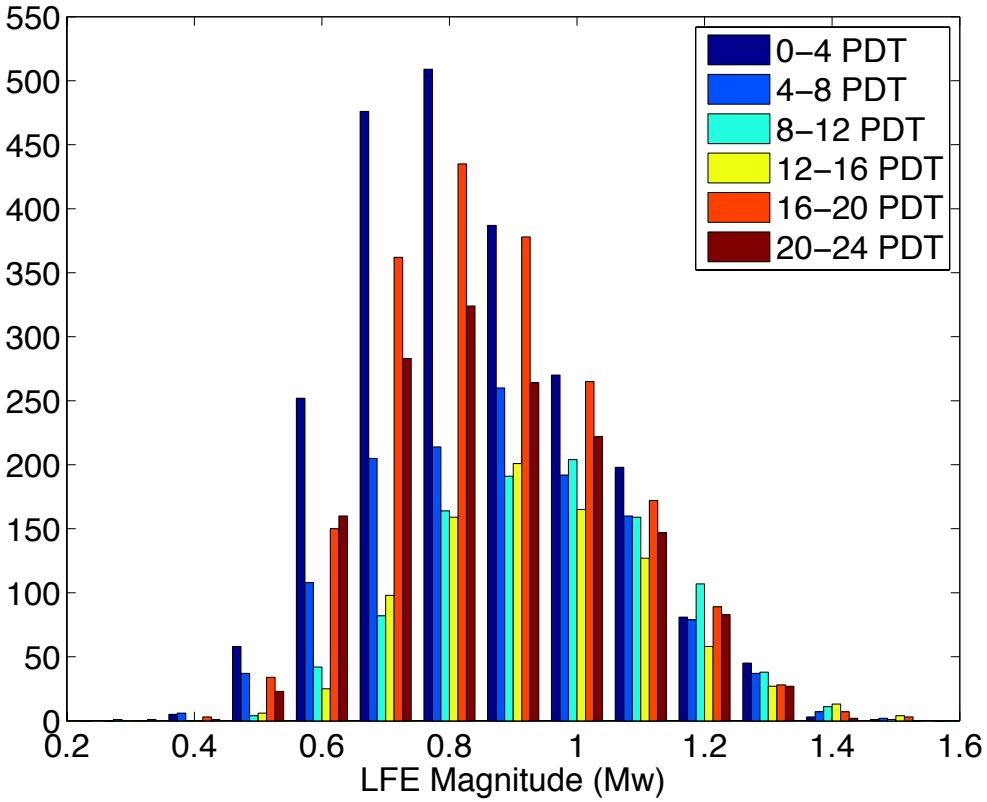

Figure 3.S7 – Number of detected LFEs of a given moment magnitude (M_w) binned by time of detection. Note that for M_w>=1.0 the number of LFE detections is roughly the same at all times of the day. Below magnitude 1.0, detections during the workday hours (8AM-4PM local time) are suppressed, likely due to increased cultural noise.

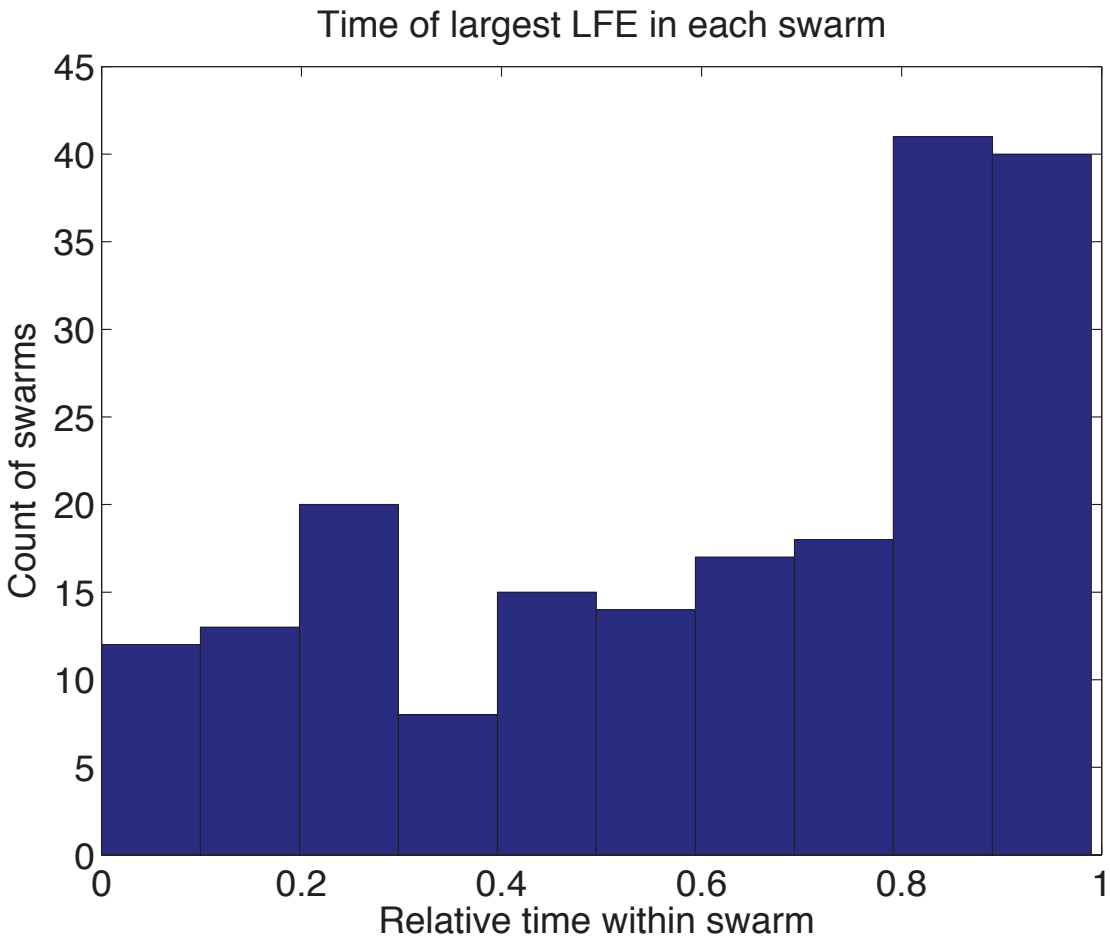

Figure 3.S8 – Histogram showing the time of the largest LFE within each swarm (0 is beginning of swarm, 1 is end of swarm). There is a clear tendency for the largest LFEs to occur near the end of swarms.

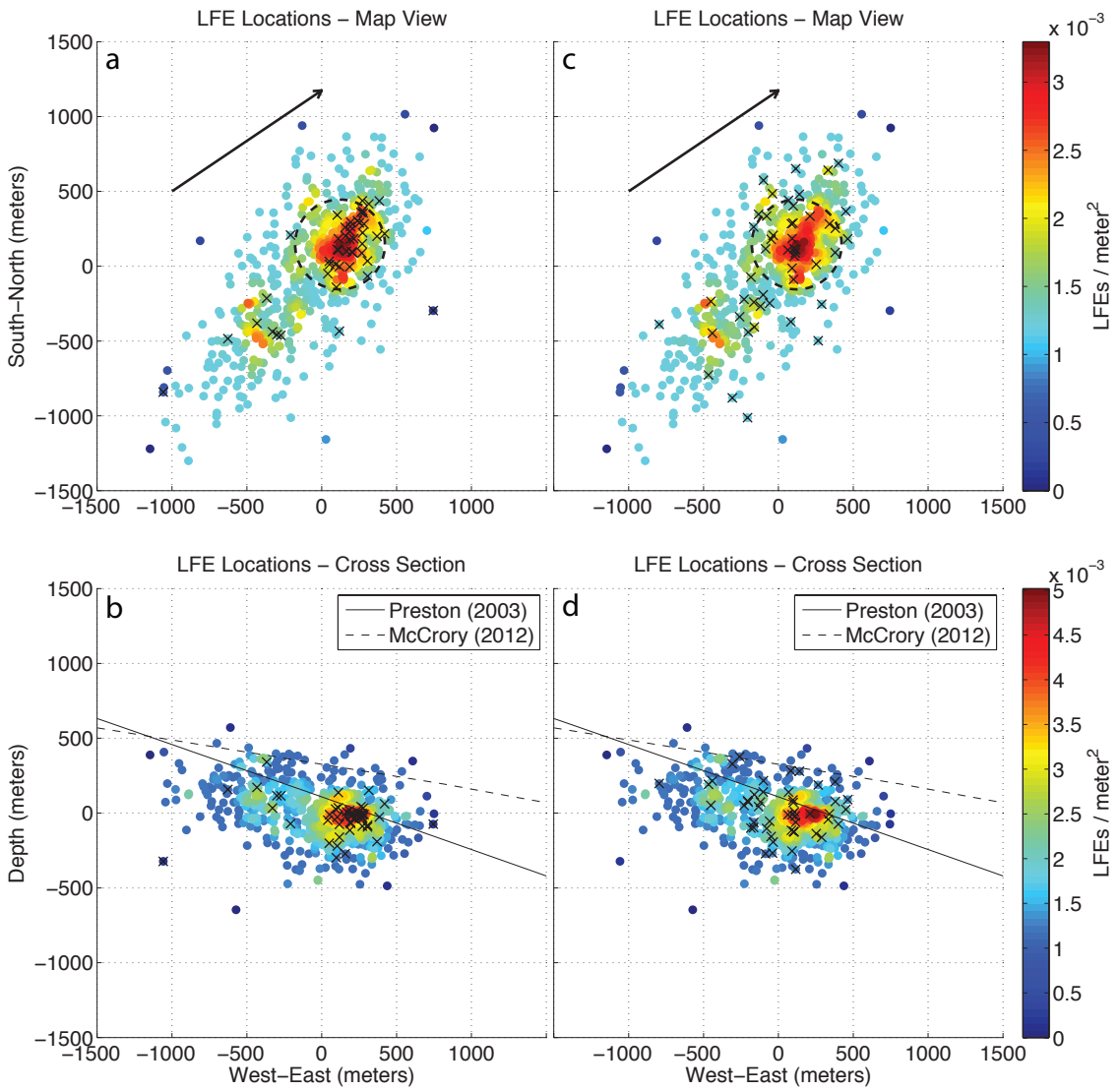

Figure 3.S9 – Locations of 700 relocated LFEs colored by density in map view (a and c) and cross section (b and d). Nearly half the LFEs lie within a 300-m radius of the patch core (dashed circle, a and c). The largest 50 LFEs (black crosses, a and b) cluster near the patch core while the 50 smallest LFEs (black crosses, c and d) are more widely distributed. LFE distribution is elongated in the direction of plate motion (black arrow, a and c) and occurs near the depths of plate interface models from *Preston et al.*, [2003] (solid line, b and d) and *McCrory et al.*, [2012] (dashed line, b and d).

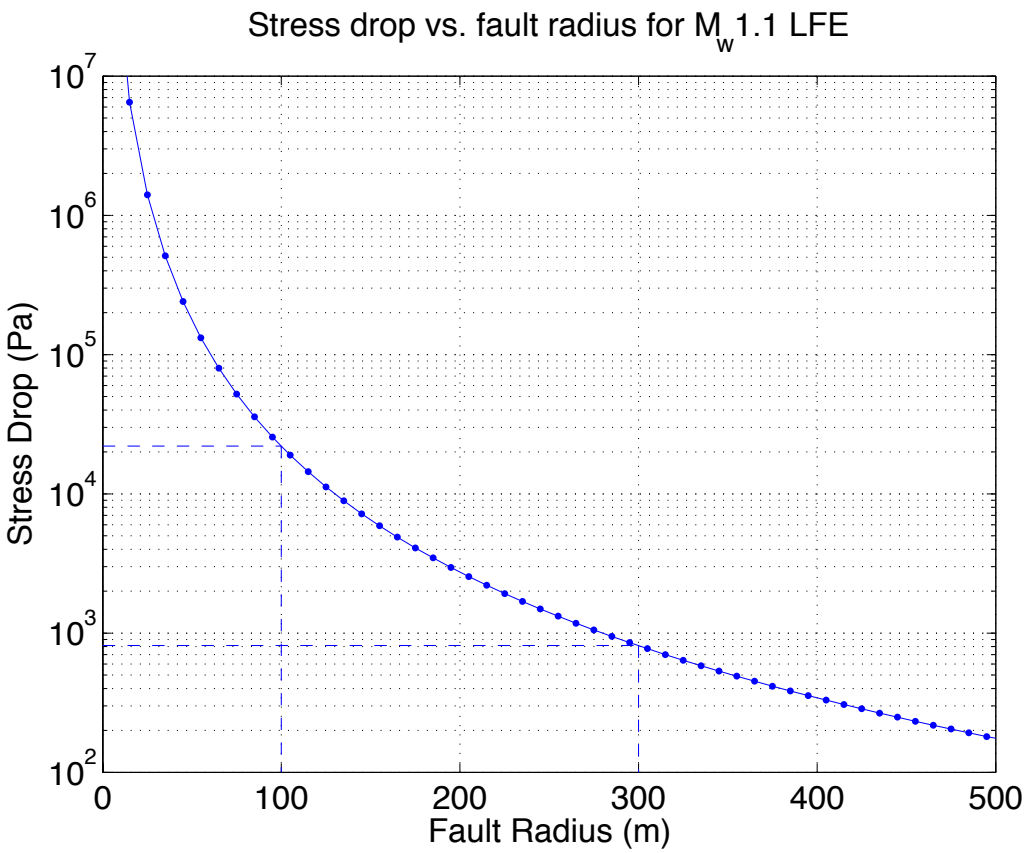

Figure 3.S10 – Plot showing the estimated stress drop for a characteristic-sized LFE (M_W1.1) for a range of circular fault radii. An LFE of this size which ruptured the entire area of our patch core (radius 300 m) would correspond to a stress drop of around ~1 kPa. If we instead use a radius of 100 m, we find a stress drop of ~20 kPa.

IV. Summary

4.1 Comparing LFE behavior in the transition zone

I have presented an analysis of four different LFE families that span the width of the transition zone in the Cascadia subduction zone beneath western Washington State. Through this analysis, I observe a systematic change in LFE amplitudes, swarm durations and swarm recurrence intervals from large values updip to small values downdip. These observations corroborate those already reported for tectonic tremor in this region [*Wech and Creager,* 2010] and further constrain the depths of tremor and LFEs to very near the location of several plate interface models. Under the likely assumption that LFEs represent small amounts of slip on the plate interface in the plate convergence direction [*Ide et al., 2007; Royer and Bostock,* 2013], our LFE observations support a friction-controlled stress transfer model that is loaded by steady creep at the downdip edge of the transition zone, with each swarm of LFEs representing a local slow slip event that transfers stress updip to adjacent portions of the plate interface. For LFE families that are active during both ETS and inter-ETS events, the significantly larger LFE amplitudes and swarm durations seen during ETS events indicate that these slip events contain larger amounts of slip. Focusing on our most updip family, we used detailed time histories to identify the passage of slow slip fronts, followed by short-duration bursts that may be tied to rapid tremor reversals (RTRs) back propagating from the slip front. The strong tidal correlation of these later short bursts indicates that the plate interface is very weakly coupled in the days following the passage of the slip front. Lastly, using two nearby LFE families, we demonstrated a method for finding

new LFE families from simultaneous, low-correlating detections in existing LFE catalogs. Double difference relocations of one of these new families indicate that it lies midway between the two existing LFE families used to discover it.

4.2 Detailed analysis of a single LFE family

Focusing on a single, isolated LFE family, I performed a number of analyses to characterize LFE patch dimensions, seismic moment, locking efficiency and stress drop. I showed that more than half the LFEs in the family clustered into a circular patch of 300 m radius. Within this patch, I further demonstrated that LFE locking efficiency was at most 20% in two 50 m radius patches, which could be responsible for the majority of the moment release seen in the larger 300 m patch. The distribution of LFE locations—elongated parallel to the plate convergence direction, and with a greater density of locations on the downdip end—led us to propose that a subducted seamount on the downgoing plate could be responsible for generating the LFEs while adjacent areas slipped aseismically. We used two estimates of patch size and an LFE of characteristic moment magnitude to constrain the range of stress drop to 1-20 kPa. We noted that LFEs rarely occurred alone, and were almost entirely clustered into swarms that occurred on average every 8 days. Surprisingly, we found that these swarms were time-predictable—meaning that the size of a given swarm could be used to predict how long it would be until the initiation of the next swarm. This type of occurrence could result from a constant stress failure threshold and the location of the LFE family we analyzed—at the very downdip edge of the transition zone and very near the stable loading of the continuously creeping zone. Within swarms we found that the largest individual LFEs usually occurred

near the end of a swarm, suggesting that smaller events in the early part of a swarm may be required to fully unlock the LFE patch for failure in large LFEs towards the end of a swarm.

Reference list

Audet, P., M. G. Bostock, N. I. Christensen, and S. M. Peacock (2009), Seismic evidence for overpressured subducted oceanic crust and megathrust fault sealing, *Nature*, 457, 76-78, doi:10.1038/nature07650.

Audet, P., M. G. Bostock, D. C. Boyarko, M. R. Brudzinski, and R. M Allen (2010), Slab morphology in the Cascadia fore arc and its relation to episodic tremor and slip, *J. Geophys. Res*., 115, B00A16, doi:10.1029/2008JB006053.

Bartlow, N. M., S. Miyazaki, A. M. Bradley, and P. Segall (2011), Space-time correlation of slip and tremor during the 2009 Cascadia slow slip event, Geophys. Res. Lett., 38, L18309, doi:10.1029/2011GL048714.

Bostock, M. G., A. A. Royer, E. H. Hearn, and S. M. Peacock (2012), Low frequency earthquakes below southern Vancouver Island, *Geochem. Geophys. Geosyst*., 13, Q11007, doi:10.1029/2012GC004391.

Brown, J. R., G. C. Beroza, S. Ide, K. Ohta, D. R. Shelly, S. Y. Schwartz, W. Rabbel, M. Thorwart, and H. Kao (2009), Deep low frequency earthquakes in tremor localize to the plate interface in multiple subduction zones, *Geophys. Res. Lett*., 36, L19306, doi:10.1029/2009GL040027.

Brudzinski, M. R., and R. M. Allen (2007), Segmentation in episodic tremor and slip all along Cascadia, *Geology,* 35(10), 907-910.

Brune, J. N. (1970), Tectonic stress and the spectra of seismic shear waves from earthquakes, *J. Geophys. Res*., 75, 4997-5009, doi: 10.1029/JB075i026p04997.

Colella, H. V., J. H. Dieterich, K. Richards-Dinger, and A. M. Rubin (2012), Complex characteristics of slow slip events in subduction zones reproduced in multi-cycle simulations, *Geophys. Res. Lett*., 39, L20312, doi:10.1029/2012GL053276.

Dragert, H., et al. (2001), A silent slip event on the deeper Cascadia subduction subduction zone, *Science, 292,*1525-1528.

Dragert, H., and K. Wang (2011), Temporal evolution of an episodic tremor and slip event along the northern Cascadia margin, *J. Geophys. Res*., 116, B12406, doi:10.1029/2011JB008609.

Ghosh, A., J.E. Vidale, J.R. Sweet, K.C. Creager, A.G. Wech, H. Houston, E. Brodsky (2010), Rapid, continuous streaking of tremor in Cascadia, *Geochem. Geophys. Geosyst*., Q12010, doi:10.1029/2010GC003305.

Ghosh, A., J. E. Vidale, and K. C. Creager (2012), Tremor asperities in the transition zone control evolution of slow earthquakes, *J. Geophys. Res*., 117, B10301,

doi:10.1029/2012JB009249.

Gomberg, J., J. L. Rubinstein, Z. Peng, K. C. Creager, J. E. Vidale, and P. Bodin (2008), Widespread Triggering of Non-volcanic Tremor in California, *Science*, v. 319, p. 173, doi:10.1126/science.1149164.

Gomberg, J., K. Creager, J. Sweet, J. Vidale, A. Ghosh, and A. Hotovec (2012), Earthquake spectra and near-source attenuation in the Cascadia subduction zone, *J. Geophys. Res*., 117, B05312, doi:10.1029/2011JB009055.

Hanks, T. C. and H. Kanamori (1979), A moment magnitude scale, *J. Geophys. Res*., 84, B5, 2348-2350, doi:10.1029/JB084iB05p02348.

Houston, H., B. G. Delbridge, A. G. Wech, and K. C. Creager (2011), Rapid tremor reversals in Cascadia generated by a weakened plate interface, *Nature Geosci.*, 4, 404-409, doi:10.1038/ngeo1157.

Ide, S., D. R. Shelly, and G. C. Beroza (2007), Mechanism of deep low frequency earthquakes: Further evidence that deep non-volcanic tremor is generated by shear slip on the plate interface, *Geophys. Res. Lett*., 34, L03308, doi:10.1029/2006GL028890.

Ide, S., K. Imanishi, Y. Yoshida, G. C. Beroza, and D. R. Shelly (2008), Bridging the gap between seismically and geodetically detected slow earthquakes, *Geophys. Res. Lett.,* 35, 10, 6, doi: 10.1029/2008GL034014.

Ito, Y., and K. Obara (2006), Very low frequency earthquakes within accretionary prisms are very low stress-drop earthquakes, *Geophys. Res. Lett.*, 33, 9, doi: 10.1029/2006GL025883.

Kao, H., S.-J. Shan, H. Dragert, G. Rogers, J. F. Cassidy, K. Wang, T. S. James, and K. Ramachandran (2006), Spatial-temporal patterns of seismic tremor in northern Cascadia, *J. Geophys. Res*., 111, B03309, doi:10.1029/2005JB003727.

Kaproth, B. M., and C. Marone (2013), Slow earthquakes, preseismic velocity changes, and the origin of slow frictional stick-slip, *Science*, 341, 6151, 1229-1232, doi:10.1126/science.1239577.

La Rocca, M., K.C. Creager, D. Galluzzo, S. Malone, J.E. Vidale, J.R. Sweet, and A.G. Wech (2009), Cascadia tremor located near plate interface constrained by S minus P wave times, *Science*, 323, 620-623, doi:610.1126/science.116711.

McCaffrey, R., A. I. Qamar, R. W. King, R. Wells, G. Khazaradze, C. A. Williams, C. W. Stevens, J. J. Vollick, and P. C. Zwick (2007), Fault locking, block rotation and crustal deformation in the Pacific Northwest, *Geophys. J. Int*., 169, 1315-1340, doi: 10.1111/j.1365-246X.2007.03371.x.

McCrory, P. A., J. L. Blair, F. Waldhauser, and D. Oppenheimer (2012), Juan de Fuca slab geometry and its relation to Wadati-Benioff zone seismicity, *J. Geophys. Res*.: Solid Earth, 117, doi: 10.1029/2012JB009407.

Miller, M. M., T. I. Melbourne, D. J. Johnson, and W. Q. Sumner (2002), Periodic slow earthquakes from the Cascadia subduction zone, *Science, 295,* 2423, doi: 10.1126/science.1071193.

Obara, K. (2002), Nonvolcanic deep tremor associated with subduction in southwest Japan, *Science*, 296, 1679–1681, doi:10.1126/science.1070378.

Obara, K., Hirose, H., Yamamizu, F., and Kasahara, K. (2004), Episodic slow slip events accompanied by non-volcanic tremors in southwest Japan subduction zone. *Geophys. Res. Lett*. 31, doi:10.1029/2004GL020848.

Preston, L. A., K. C. Creager, R. S. Crosson, T. M. Brocher, A. M. Trehu (2003), Intraslab Earthquakes: Dehydration of the Cascadia Slab, *Science*, 302, 1197-1200, doi: 10.1126/science.1090751.

Rogers, G., and H. Dragert (2003), Episodic tremor and slip on the Cascadia subduction zone: The chatter of silent slip, *Science*, 300, 1942–1943, doi:10.1126/science.1084783.

Royer, A. A., and M. G. Bostock (2013), A comparative study of low frequency earthquake templates in northern Cascadia, *Earth and Planet. Sci. Lett*., 402, 247-256, doi:10.1016/j.epsl.2013.08.040.

Rubin, A. M. (2011), Designer friction laws for bimodal slow slip propagation speeds, *Geochem. Geophys. Geosyst*., 12, Q04007, doi:10.1029/2010GC003386.

Rubin, A. M., and J. G. Armbruster (2013), Imaging slow slip fronts in Cascadia with high precision cross-station tremor locations, *Geochem. Geophys. Geosyst*., 14, 5371-5392, doi: 10.1002/2013GC005031.

Rubinstein, J. L., J. E. Vidale, J. Gomberg, P. Bodin, K. C. Creager and S. D. Malone, (2007), Non-volcanic tremor driven by large transient shear stresses, *Nature*, 448, 579-582.

Rubinstein, J.L., M. La Rocca, J.E. Vidale, K.C. Creager, A.G. Wech (2008), Tidal Modulation of Non-Volcanic Tremor, *Science*, 319, 186, doi: 10.1126/science.1150558.

Satake, K., K. Shimazaki, Y. Tsuji, and K. Ueda (1996), Time and size of a giant earthquake in Cascadia inferred from Japanese tsunami records of January 1700, *Nature*, 379, 246-249, doi:10.1038/379246a0.

Schmidt, D. A., and H. Gao (2010), Source parameters and time-dependent slip distributions of slow slip events on the Cascadia subduction zone from 1998 to 2008, J. Geophys. Res., 115, B00A18, doi:10.1029/2008JB006045.

Shearer, P. M. (1999), *Introduction to seismology*, pp. 182-191, Cambridge University Press, New York, NY.

Shearer, P. M., G. A. Prieto, and E. Hauksson (2006), Comprehensive analysis of earthquake source spectra in southern California, *J. Geophys. Res*., 111, B06303, doi:10.1029/2005JB003979.

Shelly, D. R., G. C. Beroza, S. Ide, and S. Nakamula (2006), Low-frequency earthquakes in Shikoku, Japan and their relationship to episodic tremor and slip, *Nature*, 442, 188–191, doi:10.1038/nature04931.

Shelly, D. R., G. C. Beroza, and S. Ide (2007), Non-volcanic tremor and low frequency earthquake swarms, *Nature*, 446, 305–307, doi:10.1038/nature05666.

Shelly, D. R., W. L. Ellsworth, T. Ryberg, C. Haberland, G. S. Fuis, J. Murphy, R. M. Nadeau, and R. Bürgmann (2009), Precise location of San Andreas Fault tremors near Cholame, California using seismometer clusters: Slip on the deep extension of the fault?, *Geophys. Res. Lett.*, 36, L01303, doi:10.1029/2008GL036367.

Shelly, D. R. (2010), Periodic, chaotic, and doubled earthquake recurrence intervals on the deep San Andreas Fault, *Science*, 328, 1385-1388, doi:10.1126/science.1189741.

Shelly, D. R. and J. L. Hardebeck (2010), Precise tremor source locations and amplitude variations along the lower-crustal central San Andreas Fault, *Geophys. Res. Lett*., 37, L14301, doi:10.1029/2010GL043672.

Sweet, J. R., K. C. Creager, and H. Houston (2014), A family of repeating low-frequency earthquakes at the downdip edge of tremor and slip, *Geochem. Geophys. Geosyst*., 15, doi:10.1002/2014GC005449.

Thomas, T. W., J. E. Vidale, H. Houston, K. C. Creager, J. R. Sweet, and A. Ghosh (2013), Evidence for tidal triggering of high-amplitude rapid tremor reversals and tremor streaks in northern Cascadia, *Geophys. Res. Lett*., 40, 4254–4259, doi:10.1002/grl.50832.

Waldhauser, F. and W. L. Ellsworth (2000), A double-difference earthquake location algorithm; method and application to the northern Hayward Fault, California, *Bulletin of the Seismological Society of America*, 90(6): 1353-1368.

Wang, K., H. Dragert, H. Kao, and E. Roeloffs (2008), Characterizing an "uncharacteristic" ETS event in northern Cascadia, Geophys. Res. Lett., 35, L15303, doi:10.1029/2008GL034415.

Watanabe, T., Y. Hiramatsu, and K. Obara (2007), Scaling relationship between the duration and the amplitude of non-volcanic deep low-frequency tremors, *Geophys. Res. Lett*., 34, L07305, doi:10.1029/2007GL029391.

Wech, A. G., K. C. Creager and T. I. Melbourne (2009), Seismic and geodetic constraints on Cascadia slow slip, *J. Geophys. Res*., 114, B10316, doi:10.1029/2008JB006090, 1-9.

Wech, A.G. (2010), Interactive Tremor Monitoring, *Seis. Res. Lett*., 81:4, p. 664-669.

Wech, A. G. and K. C. Creager (2011), A continuum of stress, strength and slip in the Cascadia subduction zone, *Nature GeoSci*., 4, doi:10.1038/ngeo121.